

Revisiting the role of cosmic-ray driven Alfvén waves in pre-existing magnetohydrodynamic turbulence

I. Turbulent damping rates and feedback on background fluctuations

Silvio Sergio Cerri

Université Côte d'Azur, Observatoire de la Côte d'Azur, CNRS, Laboratoire Lagrange, France
e-mail: silvio.cerri@oca.eu

May 14, 2024

ABSTRACT

Context. Alfvén waves (AWs) excited by the cosmic-ray (CR) streaming instability (CRSI) are a fundamental ingredient for CR confinement. The effectiveness of such “self-confinement” relies on a balance between CRSI growth rate and the damping mechanisms acting on quasi-parallel AWs excited by CRs. One relevant mechanism is the so-called “turbulent damping”, in which an AW packet injected in pre-existing turbulence undergoes a cascade process due to its nonlinear interaction with fluctuations of the background.

Aims. The turbulent damping of an AW packet in pre-existing magnetohydrodynamic (MHD) turbulence is re-examined, revised, and extended to include most-recent theories of MHD turbulence that account for dynamic alignment and reconnection-mediated regime. The case in which the role of feedback of CR-driven AWs on pre-existing turbulence is important will also be discussed.

Methods. The so-called Elsässer formalism is employed. Particular attention is given to the role of a “nonlinearity parameter” χ^w that estimates the strength of the nonlinear interaction between CR-driven AW packets and the background fluctuations. We point out the difference between χ^w and the parameter χ^z that instead describes the intrinsic strength of nonlinear interactions between pre-existing fluctuations. Turbulent damping rates of quasi-parallel AW packets and cosmic-ray feedback (CRF) are derived within this formalism.

Results. When the strength of nonlinear interaction is properly taken into account, one finds that (i) the turbulent damping rate of quasi-parallel AWs in sub-Alfvénic turbulence depends on the background-fluctuations' amplitude to the third power, hence is strongly suppressed, and (ii) the dependence on the AW's wavelength (and thus on the CR gyro-radius from which it is excited) is different from what has been previously obtained. Finally, (iii) when dynamic alignment of cascading fluctuations and the possibility of a reconnection-mediated range is included in the picture, the turbulent damping rate exhibits novel regimes and breaks. Finally, a criterion for CRF is derived and a simple phenomenological model of CR-modified scaling of background fluctuations is provided.

Key words. turbulence – magnetohydrodynamics – cosmic rays

1. Introduction

Turbulent, magnetized plasmas permeates a wide range of space and astrophysical environments (e.g., Quataert and Gruzinov 1999; Schekochihin and Cowley 2006; Brandenburg and Lazarian 2013; Bruno and Carbone 2013; Ferrière 2020). Understanding the properties of the turbulent cascade – how fluctuations' energy is transferred from injection to dissipation scales, thus heating the plasma and also producing non-thermal particles in the process – is a relevant task by itself, since it can elucidate the role that turbulence plays in the dynamics and thermodynamics of several astrophysical systems. In fact, inspired by the seminal work of Kolmogorov (1941) in hydrodynamics, turbulence in magnetized plasmas has been the object of several theoretical efforts aimed at obtaining universal scaling for its fluctuations at large (“fluid”) magnetohydrodynamic (MHD) scales (e.g., Iroshnikov 1963; Kraichnan 1965; Goldreich and Sridhar 1995; Ng and Bhattacharjee 1997; Galtier et al. 2000; Cho and Lazarian 2002; Boldyrev 2006; Lazarian et al. 2012; Chandran et al. 2015; Mallet et al. 2015; Boldyrev and Loureiro 2017; Mallet et al. 2017; Cerri et al. 2022; Schekochihin 2022). At the same time, these astrophysical environments are also populated with cosmic rays (CRs), i.e., charged particles with supra-thermal (relativistic) energies that pervades the interstellar, intergalac-

tic, and intracluster media (e.g., Brunetti and Jones 2014; Amato and Blasi 2018; Faucher-Giguère and Oh 2023; Ruszkowski and Pfrommer 2023) and get scattered by magnetic-field fluctuations (Ginzburg and Syrovatskii 1964; Berezhinsky et al. 1990). While cosmic-ray transport partly depends upon the properties of pre-existing turbulence (e.g., Schlickeiser and Miller 1998; Chandran 2000; Lerche and Schlickeiser 2001; Yan and Lazarian 2002, 2008; Teufel et al. 2003; Shalchi and Schlickeiser 2004; Fornieri et al. 2021; Lazarian and Xu 2021; Lemoine 2023; Kempfski et al. 2023), CRs can also generate their own scattering fluctuations through streaming instabilities (e.g., Kulsrud and Pearce 1969; Lee 1972; Skilling 1975; Gary 1993; Bell 2004; Amato 2011; Weidl et al. 2019a,b; Marcowith et al. 2021). The level at which self-generated fluctuations saturate depends on a balance between the instability growth and the damping mechanisms that these waves are subject to. Depending on the Galactic environment, the damping processes that have been originally considered are the ion-neutral (IN) damping (Kulsrud and Pearce 1969) and the non-linear Landau (NLL) damping (Lee and Völk 1973). These cosmic-ray driven Alfvén-wave (AW) packets, however, will also interact with pre-existing fluctuations of the turbulent environment in which they are generated. This interaction has been suggested to represent another source of damping, i.e., the so-called “turbulent damping”, a process for which a

CR-generated AW packet is cascaded to dissipation by its nonlinear interaction with background fluctuations. This damping mechanism was originally proposed by [Farmer and Goldreich \(2004\)](#), and subsequently extended by [Lazarian \(2016\)](#) to account for different regimes of background turbulence. However, an important parameter that has not been taken into account in these previous works is the strength of the nonlinear interaction (usually referred to as “nonlinearity parameter” χ) between the AW packet and pre-existing turbulent fluctuations. This parameter is indeed different from (and typically much smaller than) the nonlinear parameter describing the regime of background turbulence, which also needs to be taken into account (as done by [Lazarian 2016](#)). We will show that taking this difference into account completely changes the estimate of the turbulent damping rate—which is indeed almost always much lower than any rate derived previously. Moreover, such damping rate and its scaling strongly depends upon the properties of background turbulence. In the previous literature, only what we can call “classic” theories of MHD turbulence have been taken into account, i.e., isotropic Kolmogorov-like turbulence ([Kolmogorov 1941](#), hereafter “K41”), a weak cascade of Alfvénic fluctuations ([Ng and Bhattacharjee 1997](#); [Galtier et al. 2000](#), hereafter “W0”), and a critically balanced Alfvénic cascade à la [Goldreich and Sridhar \(1995\)](#) (hereafter, “GS95”). However, advanced theories of MHD turbulence that extend the above “classic” picture have been formulated in the past years. This is the case, for instance, of a theory that incorporates “dynamic” (i.e., scale-dependent) alignment of fluctuations in a critically balanced Alfvénic cascade ([Boldyrev 2006](#), hereafter “B06”), which can intrinsically lead at even smaller scales to a regime usually referred to as “tearing-mediated turbulence” (i.e., a regime where magnetic reconnection mediates the generation of smaller-scale fluctuations, [Boldyrev and Loureiro 2017](#); [Mallet et al. 2017](#), hereafter “TMT”). It is also worth mentioning that the conditions under which critical balance and the associated cascades develop (i.e., GS95, B06, and TMT regimes) may not cover all the possible scenarios in MHD turbulence (e.g., see discussion in [Oughton and Matthaeus 2020](#)). However, analytical (phenomenological) scaling of turbulent fluctuations and their anisotropy can be only derived for these cases. Moreover, several numerical simulations and *in-situ* measurements in the solar wind have provided solid evidences for these regimes (e.g., [Chen 2016](#); [Sahraoui et al. 2020](#); [Schekochihin 2022](#), and references therein). Therefore, it is of interest to derive turbulent damping rates for all these theories. The results obtained here have indeed implications for the so-called cosmic-ray “self-confinement”, since its effectiveness for CR scattering is the result of a competition between different damping mechanisms and a balance between the most-relevant damping rate and the growth rate of the CR streaming instability (e.g., [Farmer and Goldreich 2004](#); [Blasi et al. 2012](#); [Lazarian 2016](#); [Kempski and Quataert 2022](#); [Xu and Lazarian 2022](#)). For instance, by adopting the rates obtained in [Farmer and Goldreich \(2004\)](#) and [Lazarian \(2016\)](#), turbulent damping can compete with or even dominate over the IN and NLL damping processes, depending on the properties of the Galactic environment under consideration and on the CR energy (see, e.g., [Nava et al. 2019](#); [Kempski and Quataert 2022](#); [Recchia et al. 2022](#); [Xu and Lazarian 2022](#), and references therein); such picture can be significantly challenged by the new turbulent damping rates obtained here and will be addressed in detail by a following work (hereafter, “Paper II”).

The paper is organized as follows. In Section 2 the Elsässer formalism and the definitions of timescales and nonlinear parameter are introduced. In Section 3 such formalism is employed

to derive general expressions for the turbulent damping rates, whose scaling are then explicitly derived in Section 4 for various turbulent regimes and within different theories of MHD turbulence. Additionally, some considerations about the feedback of CR-driven AWs on pre-existing fluctuations and possible phenomenological models for the CR-modified background turbulent spectrum are discussed in Section 5. Finally, a summary and discussion of the results is provided in Section 6. It is worth stressing that this work is meant to primarily provide a rigorous, general formalism for deriving the turbulent damping rates of CR-driven AW packets, as well as some criterion for the possible relevance of CR feedback on pre-existing fluctuations. A more extensive discussion about different damping rates, the role of coherent structures and compressible turbulence, as well as the implications for specific astrophysical systems will be the focus of the following Paper II.

2. Setting the stage: Elsässer formalism

The magnetohydrodynamic (MHD) equations for an incompressible plasma with mass density ρ_0 , viscosity ν and resistivity η , can be conveniently expressed in terms of the Elsässer variables $z^\pm = \mathbf{u} \pm \mathbf{B}/\sqrt{4\pi\rho_0} = \mathbf{u} \pm \mathbf{v}_A$ ([Elsässer 1950](#)), where \mathbf{u} is the fluid velocity, \mathbf{B} is the magnetic field, and \mathbf{v}_A denotes the Alfvén-speed vector associated to \mathbf{B} . The incompressible MHD equations in terms of z^\pm read as

$$\frac{\partial z^\pm}{\partial t} + (z^\mp \cdot \nabla) z^\pm = -\frac{\nabla P_{\text{tot}}}{\rho_0} + \mu_+ \nabla^2 z^\pm + \mu_- \nabla^2 z^\mp, \quad (1)$$

$$\nabla \cdot z^\pm = 0, \quad (2)$$

where $P_{\text{tot}} = P_{\text{th}} + B^2/8\pi$ is the sum of the thermal and magnetic pressure and $\mu_\pm = (\nu \pm \eta)/2$. Here we assume $\nu = \eta$ for simplicity, so that $\mu_+ = \eta$ and $\mu_- = 0$. By splitting the variables into a background quantity (denoted by a “0” subscript¹) and purely transverse fluctuations, i.e., $z^\pm = z_0^\pm + \delta z_\perp^\pm$ where $z_0^\pm = \pm \mathbf{B}_0/\sqrt{4\pi\rho_0} = \pm \mathbf{v}_{A,0}$ is the Alfvén speed associated to the background magnetic field \mathbf{B}_0 and $\delta z_\perp^\pm = \delta \mathbf{u}_\perp \pm \delta \mathbf{B}_\perp/\sqrt{4\pi\rho_0}$ the fluctuating Elsässer fields, equation (1) rewrites as

$$\left(\frac{\partial}{\partial t} \mp \underbrace{v_{A,0} \nabla_\parallel}_{\omega_{\text{lin}}^\pm \sim k_\parallel^\pm v_{A,0}} + \underbrace{\delta z_\perp^\mp \cdot \nabla_\perp}_{\omega_{\text{nl}}^\pm \sim k_\perp^\pm \delta z_\perp^\mp} - \underbrace{\eta \nabla^2}_{\omega_{\text{diss}}^\pm \sim \eta k^{\pm 2}} \right) \delta z_\perp^\pm = -\frac{\nabla \delta P_{\text{tot}}}{\rho_0}, \quad (3)$$

where the parallel and perpendicular directions are defined with respect to \mathbf{B}_0 for the global equations (but will be later defined with respect to a scale-dependent mean field $\langle \mathbf{B} \rangle_k$ in a turbulent environment); we also mention that the term $\nabla \delta P_{\text{tot}}/\rho_0$ in practice contributes just as a multiplicative factor (in Fourier space) to the nonlinear term (and associated timescale) on the left-hand side.² One important feature of the formulation in (3) is that it explicitly shows that the nonlinear term $(\delta z_\perp^\mp \cdot \nabla_\perp) \delta z_\perp^\pm$ is due only to the interaction of counter-propagating Alfvén-wave packets, δz_\perp^\pm being transverse fluctuations propagating at the Alfvén speed $v_{A,0}$ in the direction of \mathbf{B}_0 , while δz_\perp^\mp are fluctuations propagating at the same speed in the direction of $-\mathbf{B}_0$.

¹ The subscript “0” formally implies a “large-scale” average procedure $\mathbf{B}_0 = \langle \mathbf{B} \rangle_L$. In the latter, $L \sim \ell_0$ will be the injection scale of turbulence.

² By taking the divergence of (3) and using the incompressibility condition $\nabla \cdot \delta z_\perp^\pm = 0$, one finds that pressure fluctuations satisfy the condition $\nabla \cdot [\nabla \delta P_{\text{tot}}] = \nabla^2 \delta P_{\text{tot}} = \rho_0 \nabla_\perp \cdot [(\delta z_\perp^\mp \cdot \nabla_\perp) \delta z_\perp^\pm]$ ([Schekochihin 2022](#)).

From (3) one can define a nonlinear parameter χ , which measures the strength of nonlinear effects with respect to the linear propagation term, namely

$$\chi^\pm \sim \frac{|(\delta z_\perp^\pm \cdot \nabla_\perp) \delta z_\perp^\pm|}{|(v_{A,0} \nabla_\parallel) \delta z_\perp^\pm|} \sim \frac{\omega_{nl}^\pm}{\omega_{lin}^\pm} \sim \frac{\tau_A^\pm}{\tau_{nl}^\pm} \sim \frac{k_\perp^\pm \delta z_k^\pm}{k_\parallel^\pm v_{A,0}}, \quad (4)$$

and involves the wave-vector components ($k_\parallel^\pm, k_\perp^\pm$) of the evolving fluctuation δz_\perp^\pm and the amplitude δz_\perp^\pm of the counter-propagating fluctuation that induces the nonlinearities on δz_\perp^\pm . In the following, this parameter will play a central role to estimate the nonlinear cascade rate (or, “turbulent damping”) of an Alfvén-wave packet interacting with background fluctuations. In particular, to obtain the correct turbulent damping rate it is necessary to make a careful distinction between (i) the nonlinear parameter χ^z characterizing counter-propagating pre-existing fluctuations, and (ii) the nonlinear parameter χ^w describing the interaction between the AW packet and background turbulence.

3. Turbulent damping of an Alfvén-wave packet

Consider an Alfvén-wave packet that is injected in an environment filled with pre-existing Alfvénic turbulence. Let δw be the initial Elsässer variable of the packet, and λ_\perp^w and λ_\parallel^w its wavelengths perpendicular and parallel to a mean-magnetic field $\langle \mathbf{B} \rangle_{\lambda^w}$ at such scales³, respectively (the corresponding wave vectors being $k_\perp^w \sim 1/\lambda_\perp^w$ and $k_\parallel^w \sim 1/\lambda_\parallel^w$). The Alfvénic fluctuations populating the turbulent background will be characterized by certain scale-dependent relations for their Elsässer amplitude $\delta z_{\lambda_\pm^z}$, their wavelength anisotropy $\lambda_\parallel^z/\lambda_\perp^z$ (for which the corresponding wave vectors can be denoted as $k_\perp^z \sim 1/\lambda_\perp^z$ and $k_\parallel^z \sim 1/\lambda_\parallel^z$), and, if allowed, for the alignment angle between $\delta z_{\lambda_\pm^z}^+$ and $\delta z_{\lambda_\pm^z}^-$, i.e., $\sin \theta_{\lambda_\pm^z}^z$. It is now instructive to derive the general relations first, leaving the explicit scaling belonging to different turbulence theories for later. Hereafter we consider the case of balanced background turbulence, and thus drop the \pm superscript everywhere for simplicity of notation.

While propagating, the AW packet will interact nonlinearly only with counter-propagating Alfvénic fluctuations of the background. In terms of Elsässer variables, the nonlinear interaction is indeed described by the term $(\delta z \cdot \nabla) \delta w$. The strength of this nonlinear interaction can then be determined by comparing the above nonlinear term with the term describing its linear propagation, $(v_{A,0} \cdot \nabla) \delta w$. The interaction between the AW packet and the pre-existing fluctuations is described by the nonlinear parameter of the packet, i.e.,

$$\chi^w \sim \frac{\tau_A^w}{\tau_{nl}^w} \sim \frac{(\lambda_\parallel^w/v_{A,0})}{(\lambda_\perp^w/\delta z_{\lambda_\perp^w})} \sim \left(\frac{\lambda_\parallel^w}{\lambda_\perp^w} \right) \left(\frac{\delta z_{\lambda_\perp^w}}{v_{A,0}} \right), \quad (5)$$

³ One can think of each component i of this mean field at scale λ as defined, for instance, by $\langle B_i \rangle_\lambda \sim \left(\int_{1/\ell_0}^{\lambda^{-1}} B_{i,k}^2 dk \right)^{1/2}$, i.e., a magnetic field that is the result of the contribution from the background field \mathbf{B}_0 plus all the fluctuations $\delta \mathbf{B}_\lambda$ at scales $\lambda' > \lambda$ such that the nonlinear timescale $\tau_{nl,\lambda'}$ over which the associated “turbulent eddy” evolves is much longer than the nonlinear evolution timescale $\tau_{nl,\lambda}$ of fluctuations at the scale λ ($v_i z, \tau_{nl,\lambda} \gg \tau_{nl,\lambda'}$ so that turbulent eddies on scales λ' appear as “frozen” over the turnover time of turbulent eddies at scale λ). Operationally, this mean field can be defined in different ways (e.g., Cho and Vishniac 2000; Cho and Lazarian 2004; Horbury et al. 2008; Wicks et al. 2010; Chen et al. 2011; Matthaeus et al. 2012; Mallet et al. 2016; Cerri et al. 2019), but what is the most-appropriate operational definition is still matter of debate (e.g., see Oughton and Matthaeus 2020).

where “local-in-scale interactions” have been assumed, so that $\delta z_{\lambda_\pm^z}$ has been substituted with $\delta z_{\lambda_\pm^w}$ in the timescale associated to the nonlinear interaction between the AW packet and pre-existing turbulence, i.e., $\tau_{nl}^w \sim \lambda_\perp^w/\delta z_{\lambda_\pm^z} \sim \lambda_\perp^w/\delta z_{\lambda_\pm^w}$. A parameter $\chi^w \geq 1$ means strong nonlinear interactions, while $\chi^w < 1$ denotes the weakly nonlinear regime. We stress that the parameter in (5) is different from the nonlinear parameter that characterizes background turbulence, i.e., $\chi^z \sim \tau_A^z/\tau_{nl}^z \sim (\lambda_\parallel^z/\lambda_\perp^z)(\delta z_{\lambda_\pm^z}/v_{A,0})$.⁴ And we point out that, while background fluctuations can have $\chi^z \geq 1$ at scale $\lambda_\perp^z \sim \lambda_\perp^w$ (strong pre-existing turbulence), the condition $\chi^w \geq 1$ does not necessarily hold at those same scales.

In fact, one should note that χ^w is not only proportional to the amplitude of background fluctuations at the scale λ_\perp^w , i.e., $\delta z_{\lambda_\perp^w}/v_{A,0}$, but it depends also on the AW-packet’s propagation angle with respect to the mean magnetic field $\langle \mathbf{B} \rangle_{\lambda^w}$ at that scale: $\lambda_\parallel^w/\lambda_\perp^w \sim k_\perp^w/k_\parallel^w = \tan \Theta_{kB}^w$, where Θ_{kB}^w is the angle between \mathbf{k}^w and $\langle \mathbf{B} \rangle_{\lambda^w \sim 1/k^w}$. As a result, if the amplitude δz_0 of background fluctuations at injection scale ℓ_0 is such that $\delta z_0/v_{A,0} \leq 1$, then strong nonlinear interactions at scales $\lambda_\perp^w \ll \ell_0$ (where $\delta z_{\lambda_\perp^w} \ll \delta z_0$) require $\lambda_\parallel^w/\lambda_\perp^w \sim v_{A,0}/\delta z_{\lambda_\perp^w} \gg 1$. This regime is thus achieved only by quasi-perpendicular AW packets. In critically balanced pre-existing turbulence, for instance, fluctuations obey the relation $\delta z_{\lambda_\pm^z}/v_{A,0} \sim \lambda_\parallel^z(\lambda_\perp^z)/\lambda_\perp^z$. Therefore, assuming local-in-scale interactions ($\lambda_\perp^z \sim \lambda_\perp^w$), the condition $\lambda_\parallel^w/\lambda_\perp^w \sim v_{A,0}/\delta z_{\lambda_\perp^w}$ means that an AW packet undergoes strong nonlinear interactions (and thus severe turbulent damping) only if its wavevector matches the anisotropy of background turbulence associated to perpendicular scale λ_\perp^w , i.e., $\lambda_\parallel^w \approx \lambda_\parallel^z(\lambda_\perp^w)$. Therefore the nonlinear interaction between a quasi-parallel AW (characterized by $\lambda_\parallel^w/\lambda_\perp^w \ll 1$), and anisotropic pre-existing turbulence (characterized by $\lambda_\perp^z/\lambda_\parallel^z \ll 1$) is always weak, i.e., $\chi^w \ll 1$.

This can be shown explicitly by considering the quasi-parallel propagation limit, which is the case of interest for CR-generated AW packets. In this case, the propagation can only be as parallel as the external turbulence allows, i.e., the propagation angle cannot be smaller than the amount $\delta b_{\lambda^w}/\langle \mathbf{B} \rangle_{\lambda^w} \sim \delta z_{\lambda_\perp^w}/v_{A,0}$ because of the field-line distortions induced by pre-existing turbulent fluctuations δb_{λ^w} over the wavelength λ_\perp^w of the packet. Therefore, the quasi-parallel (q||) propagation limit is set by

$$\frac{\lambda_\parallel^w}{\lambda_\perp^w} \Big|_{\min} = \frac{\lambda_\parallel^{w,q||}}{\lambda_\perp^{w,q||}} \sim \frac{\delta z_{\lambda_\perp^{w,q||}}}{v_{A,0}}. \quad (6)$$

Hence, the associated nonlinear parameter in this limit is

$$\chi^{w,q||} \sim \left(\frac{\delta z_{\lambda_\perp^{w,q||}}}{v_{A,0}} \right)^2. \quad (7)$$

The strongly nonlinear regime can thus be achieved only at scales λ where the AW packet interacts with pre-existing super-Alfvénic fluctuations ($\delta z_{\lambda}/v_{A,0} > 1$). In this regime, the concept of quasi-parallel propagation in (6) does not apply because at scales where $\delta b_{\lambda^w}/\langle \mathbf{B} \rangle_{\lambda^w} > 1$, the distinction between λ_\perp^w and λ_\parallel^w is lost and $\lambda_\perp^w \sim \lambda_\parallel^w \sim \lambda$ holds; hence, $\chi^w \sim \delta z_{\lambda}/v_{A,0} \geq 1$. However, even for external turbulence that is injected with super-Alfvénic amplitude, i.e., $\delta z_0/v_{A,0} \approx M_{A,0} > 1$ at scale ℓ_0 , the fluctuations’ amplitude will decrease with decreasing scale. As a result, the nonlinear interaction between the AW and external fluctuations will become weak at “small-enough” scales, i.e. at

⁴ Or, if scale-dependent (“dynamic”) alignment is taken into account, it is $\chi^z \sim \sin \theta_{\lambda_\pm^z}^z (\lambda_\parallel^z/\lambda_\perp^z)(\delta z_{\lambda_\pm^z}/v_{A,0})$ (see Appendix A).

scales $\lambda_{\perp}^w < \ell_A = \ell_0/M_{A,0}^3 \ll \ell_0$ for which the initially super-Alfvénic fluctuations become sub-Alfvénic, $\delta z_{\lambda_{\perp}^w}/v_{A,0} < 1$, and anisotropic (see Appendix A). Another way to visualize this is by rewriting (7) as

$$\chi^{w,\text{qll}} \sim \left(\frac{\lambda_{\perp}^z}{\lambda_{\parallel}^z} \right)^2 (\chi^z)^2, \quad (8)$$

which is $\ll \chi^z$ for anisotropic background fluctuations, $\lambda_{\perp}^z \ll \lambda_{\parallel}^z$, and thus $\chi^{w,\text{qll}} \ll 1$ even if pre-existing turbulence is critically balanced ($\chi^z \sim 1$).

The difference between the intrinsic nonlinear parameter of background fluctuations (χ^z) and the nonlinear parameters of a quasi-parallel Alfvén wave interacting with those fluctuations (χ^w) for explicit MHD turbulent scaling in different regimes is reported the last two columns Table 1.

Having clarified the packet’s nonlinear regimes that have to be considered in terms of background turbulence, we can now estimate the associated rate of “turbulent damping”. This means estimating the timescale over which such AW packet undergoes a cascade process due to its nonlinear interaction with pre-existing turbulent fluctuations. The cascade time of the packet is given by $\tau_{\text{casc}}^w \sim (\tau_{\text{nl}}^w)^2/\tau_A^w \sim \tau_{\text{nl}}^w/\chi^w$ for the weak regime ($\chi^w < 1$), while it is $\tau_{\text{casc}}^w \sim \tau_{\text{nl}}^w$ in the strongly nonlinear case ($\chi^w \gtrsim 1$, which we recall also implies that $\lambda_{\parallel}^w \sim \lambda_{\perp}^w \sim \lambda^w$; see paragraph below (7)).

As a result, the turbulent damping rate is:

$$\Gamma_{\text{turb}}^w \sim \frac{1}{\tau_{\text{casc}}^w} \sim \begin{cases} \left(\frac{\lambda_{\perp}^w}{\lambda_{\parallel}^w} \right) \left(\frac{\lambda_{\perp}^w}{\ell_0} \right)^{-1} \left(\frac{\delta z_{\lambda_{\perp}^w}}{v_{A,0}} \right)^2 \frac{v_{A,0}}{\ell_0} & \text{if } \chi^w < 1 \\ \left(\frac{\lambda_{\perp}^w}{\ell_0} \right)^{-1} \left(\frac{\delta z_{\lambda_{\perp}^w}}{v_{A,0}} \right) \frac{v_{A,0}}{\ell_0} & \text{if } \chi^w \gtrsim 1 \end{cases} \quad (9)$$

which reduces to

$$\Gamma_{\text{turb}}^{w,\text{qll}} \sim \left(\frac{\lambda_{\perp}^{w,\text{qll}}}{\ell_0} \right)^{-1} \left(\frac{\delta z_{\lambda_{\perp}^{w,\text{qll}}}}{v_{A,0}} \right)^3 \frac{v_{A,0}}{\ell_0} \quad (10)$$

for quasi-parallel propagation and $\chi^{w,\text{qll}} < 1$. (We recall that χ^w should not be identified with the nonlinear parameter χ^z that describes the strength of background turbulence). Therefore, when $\chi^w < 1$ the turbulent damping rate of an AW packet is nonlinear with respect to the background-fluctuations’ amplitude and depends on the propagation angle of the wave, becoming a third-order quantity of the pre-existing turbulent amplitude in the quasi-parallel limit.

We conclude by highlighting that in (10) there is a λ_{\perp}^{-1} in front of the $\delta z_{\lambda_{\perp}^z}^3$ term. Therefore, a turbulent perpendicular scaling for $\delta z_{\lambda_{\perp}^z} \propto \lambda_{\perp}^{\alpha}$ with a spectral index $\alpha > 1/3$ will produce a turbulent damping rate of quasi-parallel AW packets that decreases with decreasing scale. That would be the case of weak Alfvénic turbulence as in Galtier et al. (2000) or the tearing-mediated regime in Boldyrev and Loureiro (2017) and Mallet et al. (2017). On the other hand, fluctuations that scale with $\alpha < 1/3$ will result in a damping rate that increases with decreasing λ_{\perp}^z . This would be the case of critically balanced, strong Alfvénic turbulence with scale-dependent alignment as in Boldyrev (2006). Finally, for a Kolmogorov-like perpendicular scaling $\delta z_{\lambda_{\perp}^z} \propto \lambda_{\perp}^{1/3}$ as in critically balanced strong Alfvénic turbulence without dynamic alignment (Goldreich and Sridhar 1995), we can expect that the turbulent damping of quasi-parallel AW packets becomes scale-independent, i.e., $\Gamma_{\text{GS95}}^{w,\text{qll}} \sim \text{const.}$

4. Turbulent damping with explicit MHD scalings

The injection-scale Alfvénic Mach number is defined as the ratio $M_{A,0} \approx \delta z_0/v_{A,0}$, where δz_0 is the fluctuations’ amplitude at injection scale ℓ_0 , and determines the cascading regimes of background fluctuations. The Lundquist number at injection scale, $S_0 = \ell_0 v_{A,0}/\eta$, is related to the system’s resistivity η and determines the dissipation scale of turbulent fluctuations (we remind that here we have assumed $\nu = \eta$). If we assume isotropic injection, the nonlinear parameter of background turbulence at scale ℓ_0 indeed corresponds to the injection-scale Alfvénic Mach number, $\chi_0^z \approx M_{A,0}$. If $M_{A,0} < 1$ turbulence is called “sub-Alfvénic”: it starts as an anisotropic weak cascade that transitions into critically balanced, strong turbulence at smaller scales (still anisotropic, but in a different fashion). “Trans-Alfvénic” turbulence ($M_{A,0} \approx 1$) consists of an anisotropic strong cascade of critically balanced fluctuations at all scales. When $M_{A,0} > 1$ (large-amplitude injection), turbulence is called “super-Alfvénic” and fluctuations initially undergo an isotropic (“hydrodynamic-like”) cascade until sub-Alfvénic amplitudes are attained at smaller scales, and turbulence becomes critically balanced and anisotropic. Then, if scale-dependent (“dynamic”) alignment of fluctuations is allowed in the critical-balance range, an additional transition to a different regime of anisotropic, strong turbulence can occur at even smaller scales due to magnetic reconnection (if the injection-scale Lundquist number S_0 is large enough; see Section 4.2). In the following we only summarize the relevant scaling of background turbulent fluctuations in the different ranges. These scaling relations, along with the intrinsic nonlinear parameter χ^z of background fluctuations and the nonlinear parameter χ^w of a quasi-parallel AW propagating through such background turbulence, are also reported in Table 1 for convenience. A more detailed derivation of these ranges and of the associated scaling is provided in Appendix A.

The turbulent damping rates of this Section are derived as follows:

1. We employ the known perpendicular scaling of background turbulence, $\delta z_{\lambda_{\perp}^z}$, and locality of interactions ($\lambda_{\perp}^z \sim \lambda_{\perp}^{w,\text{qll}}$) in (10) to obtain the turbulent damping rate as a function of the packet’s perpendicular wavelength, $\Gamma_{\text{turb}}^{w,\text{qll}}(\lambda_{\perp}^{w,\text{qll}})$.
2. We use the quasi-parallel condition in (6) to retrieve the scaling of $\Gamma_{\text{turb}}^{w,\text{qll}}$ with respect to the parallel wavelength $\lambda_{\parallel}^{w,\text{qll}}$.

The scaling of the turbulent damping rate for different background cascades and the corresponding range of scales where that is valid is reported in Table 2, along with an explicit comparison with the rates available in the existing literature, i.e., from Farmer and Goldreich (2004) (“FG04”) and from Lazarian (2016) (“L16”). The behaviour of these damping rates and the comparison with previous estimates for two choices of sub-Alfvénic and super-Alfvénic injection ($M_{A,0} = 0.1, 10$) and for $S_0 = 10^{14}$ are also shown in Figure 1, for convenience. We stress that previous results not only overestimate such damping rate by a factor that could be several orders of magnitude, but in most cases they also obtain a completely different result on how this damping rate depends upon the packet’s parallel wavelength λ_{\parallel}^w .

4.1. MHD turbulence without scale-dependent alignment

We first consider the “classic” picture in which dynamic alignment of turbulent fluctuations does not occur. In this case, we have three possible regimes for background turbulence:

Quasi-parallel Alfvén waves in MHD turbulence					
background cascade (acronym)	scale range of validity		scaling of background turbulent fluctuations	nonlinear parameter of background turbulence	nonlinear parameter of quasi-parallel AWs
	$\lambda_{\perp,\max}$	$\lambda_{\perp,\min}$	$\delta z_{\lambda_{\perp}}^z$	$\chi_{\lambda_{\perp}}^z$	$\chi_{\lambda_{\perp}}^{w,\text{qll}}$
without scale-dependent alignment					
<i>sub-Alfvénic injection</i> ($M_{A,0} < 1$):					
(W0)	ℓ_0	$M_{A,0}^2 \ell_0$	$v_{A,0} M_{A,0} (\lambda_{\perp}/\ell_0)^{1/2}$	$M_{A,0} (\lambda_{\perp}/\ell_0)^{-1/2}$	$M_{A,0}^2 (\lambda_{\perp}/\ell_0)$
(GS95)	$M_{A,0}^2 \ell_0$	$M_{A,0}^{-1} S_0^{-3/4} \ell_0$	$v_{A,0} M_{A,0}^{4/3} (\lambda_{\perp}/\ell_0)^{1/3}$	~ 1	$M_{A,0}^{8/3} (\lambda_{\perp}/\ell_0)^{2/3}$
<i>trans-Alfvénic injection</i> ($M_{A,0} \approx 1$):					
(GS95)	ℓ_0	$S_0^{-3/4} \ell_0$	$v_{A,0} (\lambda_{\perp}/\ell_0)^{1/3}$	~ 1	$(\lambda_{\perp}/\ell_0)^{2/3}$
<i>super-Alfvénic injection</i> ($M_{A,0} > 1$):					
(K41)	ℓ_0	$M_{A,0}^{-3} \ell_0$	$v_{A,0} M_{A,0} (\lambda/\ell_0)^{1/3}$	$M_{A,0} (\lambda/\ell_0)^{1/3}$	$M_{A,0} (\lambda/\ell_0)^{1/3}$
(GS95)	$M_{A,0}^{-3} \ell_0$	$(M_{A,0} S_0)^{-3/4} \ell_0$	$v_{A,0} M_{A,0} (\lambda_{\perp}/\ell_0)^{1/3}$	~ 1	$M_{A,0}^2 (\lambda_{\perp}/\ell_0)^{2/3}$
with scale-dependent alignment					
<i>sub-Alfvénic injection</i> ($M_{A,0} < 1$):					
(W0)	ℓ_0	$M_{A,0}^2 \ell_0$	$v_{A,0} M_{A,0} (\lambda_{\perp}/\ell_0)^{1/2}$	$M_{A,0} (\lambda_{\perp}/\ell_0)^{-1/2}$	$M_{A,0}^2 (\lambda_{\perp}/\ell_0)$
(B06)	$M_{A,0}^2 \ell_0$	$M_{A,0}^{-2/7} S_0^{-4/7} \ell_0$	$v_{A,0} M_{A,0}^{3/2} (\lambda_{\perp}^z/\ell_0)^{1/4}$	~ 1	$M_{A,0}^3 (\lambda_{\perp}^z/\ell_0)^{1/2}$
(TMT)	$M_{A,0}^{-2/7} S_0^{-4/7} \ell_0$	$M_{A,0}^{-1} S_0^{-3/4} \ell_0$	$v_{A,0} S_0^{1/5} M_{A,0}^{8/5} (\lambda_{\perp}/\ell_0)^{3/5}$	~ 1	$S_0^{2/5} M_{A,0}^{16/5} (\lambda_{\perp}/\ell_0)^{6/5}$
<i>trans-Alfvénic injection</i> ($M_{A,0} \approx 1$):					
(B06)	ℓ_0	$S_0^{-4/7} \ell_0$	$v_{A,0} (\lambda_{\perp}/\ell_0)^{1/4}$	~ 1	$(\lambda_{\perp}/\ell_0)^{1/2}$
(TMT)	$S_0^{-4/7} \ell_0$	$S_0^{-3/4} \ell_0$	$v_{A,0} S_0^{1/5} (\lambda_{\perp}/\ell_0)^{3/5}$	~ 1	$S_0^{2/5} (\lambda_{\perp}/\ell_0)^{6/5}$
<i>super-Alfvénic injection</i> ($M_{A,0} > 1$):					
(K41)	ℓ_0	$M_{A,0}^{-3} \ell_0$	$v_{A,0} M_{A,0} (\lambda/\ell_0)^{1/3}$	$M_{A,0} (\lambda/\ell_0)^{1/3}$	$M_{A,0} (\lambda/\ell_0)^{1/3}$
(B06)	$M_{A,0}^{-3} \ell_0$	$M_{A,0}^{-9/7} S_0^{-4/7} \ell_0$	$v_{A,0} M_{A,0}^{3/4} (\lambda_{\perp}/\ell_0)^{1/4}$	~ 1	$M_{A,0}^{3/2} (\lambda_{\perp}/\ell_0)^{1/2}$
(TMT)	$M_{A,0}^{-9/7} S_0^{-4/7} \ell_0$	$(M_{A,0} S_0)^{-3/4} \ell_0$	$v_{A,0} S_0^{1/5} M_{A,0}^{6/5} (\lambda_{\perp}^z/\ell_0)^{3/5}$	~ 1	$S_0^{2/5} M_{A,0}^{12/5} (\lambda_{\perp}^z/\ell_0)^{6/5}$

Table 1: Summary of the relevant scaling relations for balanced MHD turbulence in the different regimes mentioned in Section 4 (see Appendix A for the derivation). The last two columns explicitly show the difference between the intrinsic nonlinear parameter χ^z of background fluctuations and the nonlinear parameter $\chi^{w,\text{qll}}$ of a quasi-parallel Alfvén wave interacting with those fluctuations. Note that locality of interactions $\lambda_{\perp}^w \sim \lambda_{\perp}^z \sim \lambda_{\perp}$ has been implied everywhere and that in all the regimes with dynamic alignment, a transition to a tearing-mediated range (TMT) has been assumed, i.e., that the injection-scale Lunquist number satisfies the inequality $S_0 \gg M_{A,0}^{-4}$ ($S_0 \gg M_{A,0}^3$) for sub-Alfvénic (super-Alfvénic) injection. See Table 2 for the consequences of not taking into account this difference between $\chi^{w,\text{qll}}$ and χ^z on the inferred turbulent damping rate of quasi-parallel Alfvén waves.

[W0] A weak anisotropic cascade with fluctuations' scaling $\delta z_{\lambda_{\perp}}^{(W0)}/v_{A,0} \sim M_{A,0} (\lambda_{\perp}^z/\ell_0)^{1/2}$ that only generates smaller perpendicular scales (i.e., $\lambda_{\perp}^z \sim \ell_0 \approx \text{const.}$) and transitions into a critically balanced cascade at $\lambda_{\perp,\text{CB}}^z \sim M_{A,0}^2 \ell_0$. This

cascade is realized in the range of scales $\lambda_{\perp,\text{CB}}^z \lesssim \lambda_{\perp}^z \lesssim \ell_0$, and only for sub-Alfvénic injection ($M_{A,0} < 1$).

[K41] A strong, isotropic (“hydrodynamic-like”) cascade characterized by the scaling $\delta z_{\lambda_{\perp}}^{(K41)}/v_{A,0} \sim M_{A,0} (\lambda^z/\ell_0)^{1/3}$.

These fluctuations attain sub-Alfvénic amplitudes, becoming anisotropic and critically balanced, at a scale $\ell_A \sim M_{A,0}^{-3} \ell_0$. This cascade is realized at scales $\ell_A \lesssim \lambda^z \lesssim \ell_0$, and only for super-Alfvénic injection ($M_{A,0} > 1$).

[GS95] A strong anisotropic cascade of critically balanced fluctuations with perpendicular scaling $\delta z_{\lambda_{\perp}^z}^{(\text{GS95})} \propto (\lambda_{\perp}^z)^{1/3}$. This type of cascade is realized either for trans-Alfvénic injection ($M_{A,0} \approx 1$), or when cascading fluctuations of the two above regimes reach the scale $\lambda_{\perp, \text{CB}}^z$ or ℓ_A , respectively. For trans/sub-Alfvénic injection ($M_{A,0} \lesssim 1$), the dependence on $M_{A,0}$ of the scaling is $\delta z_{\lambda_{\perp}^z}^{(\text{GS95})}/v_{A,0} \sim M_{A,0}^{4/3} (\lambda_{\perp}^z/\ell_0)^{1/3}$, and the cascade achieves dissipation at a scale $\lambda_{\perp, \text{min}}^z/\ell_0 \sim M_{A,0}^{-1} S_0^{-3/4}$. For super-Alfvénic injection ($M_{A,0} > 1$), the fluctuations' scaling with $M_{A,0}$ is linear, i.e., $\delta z_{\lambda_{\perp}^z}^{(\text{GS95})}/v_{A,0} \sim M_{A,0} (\lambda_{\perp}^z/\ell_0)^{1/3}$, and the dissipation scale is given by $\lambda_{\perp, \text{min}}^z/\ell_0 \sim (M_{A,0} S_0)^{-3/4}$. Here $S_0 = \ell_0 v_{A,0}/\eta$ is the Lundquist number at injection scale.

By using (7) one can verify that the nonlinear interaction between a quasi-parallel AW packets with wavelength $\lambda_{\perp}^{w, \text{qll}}$ and pre-existing turbulence is weak, $\chi^{w, \text{qll}} \ll 1$, in the range of scales where the cascade of background fluctuations is either weak (“W0”) or critically balanced (“GS95”). This means $\chi^{w, \text{qll}} \ll 1$ at scales $\lambda_{\perp}^{w, \text{qll}} < \ell_0$ ($\lambda_{\perp}^{w, \text{qll}} < \ell_A$) for sub-Alfvénic (super-Alfvénic) injection (see Table 1 for the explicit scaling of $\chi^{w, \text{qll}}$ in these different regimes). Hence, the cascade time $\tau_{\text{casc}}^{w, \text{qll}} \sim \tau_{\text{nl}}^w/\chi^{w, \text{qll}}$ of the AW packets for these cases is not just the nonlinear time τ_{nl}^w , and the turbulent damping rate is given by (10). In Farmer and Goldreich (2004), for instance, the nonlinear time τ_{nl}^z instead of $\tau_{\text{casc}}^{w, \text{qll}}$ has been used to compute the turbulent damping rate. In a subsequent work by Lazarian (2016), instead, the nonlinear parameter of background turbulence χ^z was used instead of $\chi^{w, \text{qll}} \ll \chi^z$ to compute a cascade time $\tau_{\text{nl}}^w/\chi^z$. This resulted in an estimated timescale for turbulent damping that can be notably shorter than the actual cascade time that should be used. Taking properly into account the difference between χ^z and $\chi^{w, \text{qll}}$ thus changes significantly the effectiveness of turbulent damping in pre-existing turbulence with respect to all these previous estimates (see Table 2 for the generic case, or Figure 1 for a two specific examples of sub- and super-Alfvénic injection regimes).

4.1.1. sub- and trans-Alfvénic turbulence ($M_{A,0} \leq 1$) without dynamic alignment

In sub-Alfvénic background turbulence without dynamic alignment, a quasi-parallel AW packet with (normalized) parallel wavelength $\hat{\lambda}_{\parallel}^w = \lambda_{\parallel}^{w, \text{qll}}/\ell_0$ is subject to the following turbulent damping rate:

$$[M_{A,0} < 1, \text{ no dynamic alignment}]$$

$$\Gamma_{\text{subA}}^{w, \text{qll}} \sim \begin{cases} M_{A,0}^{8/3} (\hat{\lambda}_{\parallel}^w)^{1/3} \frac{v_{A,0}}{\ell_0} & M_{A,0}^4 \lesssim \hat{\lambda}_{\parallel}^w \lesssim M_{A,0} \\ M_{A,0}^4 \frac{v_{A,0}}{\ell_0} & \hat{\lambda}_{\parallel, \text{min}}^{w, (\text{subA})} \lesssim \hat{\lambda}_{\parallel}^w \lesssim M_{A,0}^4 \end{cases} \quad (11)$$

where $\hat{\lambda}_{\parallel, \text{min}}^{w, (\text{subA})} \sim (M_{A,0} \hat{\lambda}_{\perp, \text{min}}^{z, (\text{subA})})^{4/3} \sim S_0^{-1}$ is the minimum packet's wavelength that is effectively subject to turbulent damping, with $\hat{\lambda}_{\perp, \text{min}}^{z, (\text{subA})} \sim M_{A,0}^{-1} S_0^{-3/4}$ being the (normalized) dissipation scale of the turbulence. The ranges of $\hat{\lambda}_{\parallel}^w$ in (11) have

been determined accordingly to the quasi-parallel condition in (6) and, assuming local interactions $\lambda_{\perp}^{w, \text{qll}} \sim \lambda_{\perp}^z$, employing the λ_{\perp}^z range of validity for each turbulent regime (see Appendix A).

The trans-Alfvénic regime is trivially obtained from (11) when the initial weak cascade does not occur:

$$[M_{A,0} \approx 1, \text{ no dynamic alignment}]$$

$$\Gamma_{\text{transA}}^{w, \text{qll}} \sim \frac{v_{A,0}}{\ell_0} (\hat{\lambda}_{\perp, \text{min}}^z)^{4/3} \lesssim \hat{\lambda}_{\parallel}^w \lesssim 1 \quad (12)$$

where $\hat{\lambda}_{\perp, \text{min}}^z \sim S_0^{-3/4}$ is the (normalized) dissipation scale of GS95 turbulence in the trans-Alfvénic regime.

The damping rates in (11) differ from what previously derived in the literature (see Table 2) because here the nonlinear parameter of the AW packet has been properly taken into account (see Table 1). In fact, one can verify that the turbulent-damping rate in the (W0) range of sub-Alfvénic turbulence, i.e., equation (46) of Lazarian (2016), can be recovered if the nonlinear parameter χ^z of background turbulence is employed instead of the nonlinear parameter χ^w of the AW packet. Analogously, the result in the (GS95) range of sub-Alfvénic turbulence in equation (34) of the same paper is recovered by assuming strong interactions between the quasi-parallel AW packet and background fluctuations, i.e., identifying χ^w with $\chi^z \sim 1$ at those scales. However, given the expression for χ^w in (5), the assumption $\chi^w \sim 1$ would require $\lambda_{\parallel}^w/\lambda_{\perp}^w \sim v_{A,0}/\delta z_{\lambda_{\perp}^w} \gg 1$, which is inconsistent with the quasi-parallel limit $\lambda_{\parallel}^w/\lambda_{\perp}^w \ll 1$. The same argument applies when comparing the damping rate for the trans-Alfvénic case in (12) with equation (9) of Farmer and Goldreich (2004).

It is important to stress that the results obtained here strongly change the effectiveness of the turbulent damping of CR-generated Alfvén-wave packets. In fact, depending on the Alfvénic Mach number $M_{A,0}$ and on the Lundquist number S_0 , the damping rates in (11)-(12) can be several orders of magnitude smaller than the ones previously derived and usually employed in CR studies (see Table 2 and the left panel in Figure 1). In particular, one can see that the damping rate of an AW packet interacting with pre-existing weak turbulence is at least a factor $M_{A,0}$ smaller than what previously estimated (i.e., at scale $\lambda_{\parallel, \text{max}}^{w, \text{qll}} \sim M_{A,0} \ell_0$, when this difference is at its minimum, then it increases even further due to the different dependence on $\lambda_{\parallel}^{w, \text{qll}}$). When the packet starts to interact with strong turbulence, i.e. for $\lambda_{\parallel, \text{CB}}^{w, \text{qll}} \sim M_{A,0}^4 \ell_0$, the damping rate becomes at least a factor $M_{A,0}^4 \ll 1$ smaller than what has been derived in the literature (a difference that, again, increases even further with decreasing packet's parallel wavelength due to the radically different wavelength dependence of $\Gamma_{\text{GS95}}^{w, \text{qll}}$ in (11)-(12) with respect to the results in Farmer and Goldreich (2004) and in Lazarian (2016)). This is indeed true also for trans-Alfvénic injection ($M_{A,0} \approx 1$), in which case the damping rate in (12) would be the same as the one in the literature only at scales $\lambda_{\parallel}^{w, \text{qll}} \sim \ell_0$, and then the two results would rapidly diverge with decreasing wavelength of the quasi-parallel AW packet at $\lambda_{\parallel}^{w, \text{qll}} < \ell_0$. Finally, the maximum difference between the damping rate obtained here and the ones found in the literature is achieved at the minimum wavelength for which this damping mechanism is effective: at $\lambda_{\parallel}^{w, \text{qll}} \sim \lambda_{\parallel, \text{min}}^w$ the actual damping rate is a factor $\sim S_0^{-1/2} M_{A,0}^2 \ll 1$ smaller than the results in Farmer and Goldreich (2004) and in Lazarian (2016); in astrophysical systems this factor can represent many orders of magnitude, since S_0 can be extremely large, e.g., larger

than 10^{20} (Priest and Forbes 2007). We also point out that in sub-Alfvénic turbulence the ordering $S_0 \gg M_{A,0}^{-4}$ is implied in order to have a significant (GS95) range (see Appendix A).

4.1.2. super-Alfvénic turbulence ($M_{A,0} > 1$) without dynamic alignment

When the injection regime of background fluctuations is super-Alfvénic, an AW packet is instead subject to a turbulent damping given by:

[$M_{A,0} > 1$, no dynamic alignment]

$$\Gamma_{\text{supA}}^{w,\text{qll}} \sim \begin{cases} M_{A,0} (\hat{\lambda}^w)^{-2/3} \frac{v_{A,0}}{\ell_0} & M_{A,0}^{-3} \lesssim \hat{\lambda}^w \lesssim 1 \\ M_{A,0}^3 \frac{v_{A,0}}{\ell_0} & \hat{\lambda}_{\parallel,\text{min}}^w \lesssim \hat{\lambda}^w \lesssim M_{A,0}^{-3} \end{cases} \quad (13)$$

where the damping rate in the range $M_{A,0}^{-3} \lesssim \hat{\lambda}^w \lesssim 1$ is obtained from the $\chi^w \gtrsim 1$ part of (9), and the shortest wavelength affected by turbulent damping is $\hat{\lambda}_{\parallel,\text{min}}^w \sim M_{A,0} (\hat{\lambda}_{\perp,\text{min}}^w)^{4/3} \sim S_0^{-1}$. We also point out that the isotropic normalized wavelength $\hat{\lambda}^w = \lambda^w / \ell_0$ enters the damping rate in the range $\ell_A \lesssim \lambda^w \lesssim \ell_0$, i.e., where the AW packet interacts with hydrodynamic-like pre-existing turbulence.

In the range $M_{A,0}^{-3} \lesssim \hat{\lambda}^w \lesssim 1$, the packet's nonlinear parameter is larger than unity (i.e., $\chi^w \approx \delta z_{\lambda} / v_{A,0}$, and $\delta z_{\lambda} / v_{A,0} > 1$ at those scales; cf. Table 1). Thus, the result obtained above for such range of scales agrees with the corresponding one provided in equation (55) of Lazarian (2016). This is a consequence of the fact that the quasi-parallel condition (6) does not apply in the range $\ell_0 \gtrsim \lambda \gtrsim \ell_A \approx M_{A,0}^{-3} \ell_0$ and the distinction between λ_{\parallel}^w and λ_{\perp}^w is lost. As a result, for local and isotropic interactions (meaning $\lambda^w \sim \lambda^z \sim \lambda$), there is no difference between the expressions for χ^w and for χ^z (see Table 1). On the other hand, at smaller scales ($\lambda^w \lesssim \ell_A$), we recover a distinction between λ_{\parallel}^w and λ_{\perp}^w because background fluctuations becomes sub-Alfvénic and anisotropic (i.e., $\delta z_{\lambda} / v_{A,0} < 1$ and $\lambda_{\perp}^z \ll \lambda_{\parallel}^z$); and the quasi-parallel condition (6) does apply again, affecting χ^w . Therefore, a quasi-parallel AW packet with $\lambda_{\parallel}^{w,\text{qll}} < \ell_A$ experiences a weak nonlinear interaction with background turbulence, i.e., $\chi_{\lambda_{\perp}}^{w,\text{qll}} \approx (\delta z_{\lambda} / v_{A,0})^2 \ll 1$ while background turbulence is critically balanced, $\chi_{\lambda_{\perp}}^z \sim 1$ (cf. equation (8) in Section 3 and Table 1). Hence, the two nonlinear parameters need not to be confused at scales below ℓ_A , and this is why the turbulent damping rate of quasi-parallel AWs that we obtain for this range of scales is again different from equation (52) of Lazarian (2016).

As for the sub-Alfvénic case discussed earlier, we stress that also for this $M_{A,0} > 1$ regime the result in (13) implies a drastic change in the effectiveness of turbulent damping for CR-generated Alfvén-wave packets. In fact, while our result agrees with the turbulent damping rate found in the literature for the range of scales $\ell_A \lesssim \lambda^w \lesssim \ell_0$, the corresponding rate at smaller scales, $\lambda_{\parallel}^{w,\text{qll}} < \ell_A$, can be several orders of magnitude smaller than the one usually employed in CR studies (see Table 2 and the right panel in Figure 1). The damping rate in (13) indeed rapidly diverges from the one given in Lazarian (2016) with decreasing wavelength of the quasi-parallel AW packet when $\lambda_{\parallel}^{w,\text{qll}} < \ell_A$, reaching its maximum difference at $\lambda_{\parallel}^{w,\text{qll}} \sim \lambda_{\parallel,\text{min}}^w$, where the actual damping rate in (13) is a factor $\sim S_0^{-1/2} M_{A,0}^{3/2} \ll 1$ smaller than the one provided in the literature (see the explicit compar-

ison in Table 2). We also point out that for super-Alfvénic injection, the ordering $S_0 \gg M_{A,0}^3$ is implied in order to have a significant (GS95) range (see Appendix A).

4.2. MHD turbulence with dynamic alignment

The ‘‘classic’’ picture presented above is now extended to the case in which counter-propagating Elsässer fields $\delta z_{\lambda_{\perp}}^+$ and $\delta z_{\lambda_{\perp}}^-$ (or, in a similar way, velocity and magnetic-field fluctuations, $\delta \mathbf{u}_{\lambda_{\perp}}$ and $\delta \mathbf{b}_{\lambda_{\perp}}$) tend to align with each other in a scale-dependent fashion (Boldyrev 2006). This ‘‘dynamic alignment’’ not only modifies the fluctuations’ scaling and anisotropy by inducing a weakening of the nonlinear interaction, but can also open the possibility of a reconnection-mediated regime at small scales (still within the MHD range of scales, not in the kinetic regime; see, e.g., Boldyrev and Loureiro 2017; Mallet et al. 2017). In this section, we consider the case when such a scale-dependent alignment occur only in critically balanced turbulent fluctuations⁵, $\chi^z \sim 1$. In this case, in addition to the (W0) and (K41) regimes of the previous Section 4.1, one can have two additional regimes for background turbulence (see also Table 1):

[B06] An anisotropic, strong cascade of critically balanced and dynamically aligned fluctuations that replaces the (GS95) regime. In this case, fluctuations’ alignment angle decreases with decreasing scale so that $\sin \theta_{\lambda_{\perp}}^z \propto (\lambda_{\perp}^z / \ell_0)^{1/4}$. For sub- and trans-Alfvénic injection ($M_{A,0} \leq 1$), the perpendicular scaling of turbulent fluctuations at scales $\lambda_{\perp}^z \lesssim \lambda_{\perp,\text{CB}}^z$, turns out to be $\delta z_{\lambda_{\perp}}^{(\text{B06})} / v_{A,0} \sim M_{A,0}^{3/2} (\lambda_{\perp}^z / \ell_0)^{1/4}$. When $S_0 \gg M_{A,0}^{-4}$, this cascade can further turn into a reconnection-mediated regime below a transition scale $\lambda_{\perp,*}^z / \ell_0 \sim M_{A,0}^{-2/7} S_0^{-4/7}$. For super-Alfvénic injection ($M_{A,0} > 1$), turbulent fluctuations at scales $\lambda_{\perp}^z \lesssim \ell_A$ follow instead a perpendicular scaling given by $\delta z_{\lambda_{\perp}}^{(\text{B06})} / v_{A,0} \sim M_{A,0}^{3/4} (\lambda_{\perp}^z / \ell_0)^{1/4}$. In this super-Alfvénic regime, a transition to reconnection-mediated turbulence may occur at a scale $\lambda_{\perp,*}^{z(\text{supA})} / \ell_0 \sim M_{A,0}^{-9/7} S_0^{-4/7}$ if $S_0 \gg M_{A,0}^3$. If $S_0 \lesssim M_{A,0}^{-4}$ ($S_0 \lesssim M_{A,0}^3$) in the sub-Alfvénic (super-Alfvénic) regime, the dissipation scale for a given regime is larger than the corresponding transition scale and the (B06) cascade does not transition into the tearing-mediated regime. When this is case, the dissipation scale is achieved at $\lambda_{\perp,\text{min}}^{z(\text{subA})} / \ell_0 \sim (M_{A,0} S_0)^{-2/3}$ in the trans/sub-Alfvénic regime, or at $\lambda_{\perp,\text{min}}^{z(\text{supA})} / \ell_0 \sim M_{A,0}^{-1} S_0^{-2/3}$ for super-Alfvénic injection.

[TMT] A strong anisotropic cascade of critically balanced and dynamically (mis-)aligned fluctuations that are generated by magnetic-reconnection processes. In this case, fluctuations scale as $\delta z_{\lambda_{\perp}}^{(\text{TMT})} \propto S_0^{1/5} (\lambda_{\perp}^z)^{3/5}$ and are subject to a scale-dependent mis-alignment given by $\sin \theta_{\lambda_{\perp}}^z \propto (\lambda_{\perp}^z / \ell_0)^{-4/5}$. For sub- and trans-Alfvénic injection ($M_{A,0} \leq 1$), the perpendicular scaling of tearing-mediated turbulent fluctuations is given by $\delta z_{\lambda_{\perp}}^{(\text{TMT})} / v_{A,0} \sim S_0^{1/5} M_{A,0}^{8/5} (\lambda_{\perp}^z / \ell_0)^{3/5}$, while in the super-Alfvénic regime ($M_{A,0} > 1$) they scale as

⁵ Addressing the case in which alignment could occur also at weak nonlinearities (Cerri et al. 2022) may be still premature at this point, and it requires to account for the alignment induced by background fluctuations on the AW packet itself. For the sake of simplicity, this case will not be treated here and will be addressed separately in a following work.

$\delta z_{\lambda_{\perp}^z}^{(\text{TMT})}/v_{A,0} \sim S_0^{1/5} M_{A,0}^{6/5} (\lambda_{\perp}^z/\ell_0)^{3/5}$. In this regime, the dissipation scale is the same as for the GS95 cascade, i.e., $\lambda_{\perp,\text{min}}^{z(\text{subA})}/\ell_0 \sim M_{A,0}^{-1} S_0^{-3/4}$ for trans/sub-Alfvénic turbulence, or $\lambda_{\perp,\text{min}}^{z(\text{supA})}/\ell_0 \sim (M_{A,0} S_0)^{-3/4}$ for super-Alfvénic injection.

One can verify that the nonlinear interaction between a quasi-parallel AW packet and the anisotropic turbulent fluctuations populating the background is weak also for these cascades, i.e., $\chi_{\lambda_{\perp}}^{w,\text{qll}} < 1$, except for the case of super-Alfvénic injection at scales $\lambda^w \gtrsim \ell_A$, where instead $\chi_{\lambda}^w \sim \chi_{\lambda}^z > 1$ holds (see Table 1).

We stress that a tearing-mediated range emerges either when $S_0 \gg M_{A,0}^{-4}$ or $S_0 \gg M_{A,0}^3$ for sub-Alfvénic or super-Alfvénic turbulence injection, respectively (see Appendix A). Even admitting a wide range of values for the injection-scale Alfvénic Mach number $M_{A,0}$, it seems reasonable to assume that these conditions would be met quite easily in many astrophysical systems. This is because the turbulent plasmas hosted by these environments are typically very weakly collisional, and thus characterized by large Lundquist numbers (see, e.g., Priest and Forbes 2007; Ji and Daughton 2011, and references therein). Nevertheless, for a TMT range to exist, 3D anisotropy of turbulent fluctuations is required. Hence, scale-dependent (“dynamic”) alignment is absolutely necessary. How and under which circumstances dynamic alignment occurs is still largely unexplored and matter of ongoing debate (see, e.g., Schekochihin 2022; Cerri et al. 2022, and references therein).

4.2.1. sub- and trans-Alfvénic turbulence ($M_{A,0} \leq 1$) with dynamic alignment

A quasi-parallel AW packet with (normalized) parallel wavelength $\hat{\lambda}_{\parallel}^w = \lambda_{\parallel}^{w,\text{qll}}/\ell_0$ injected in pre-existing sub-Alfvénic turbulence for which dynamic alignment of critically balanced fluctuations occurs is subject to the following turbulent damping rate:

[$M_{A,0} < 1$, with dynamic alignment]

$$\Gamma_{\text{subA}}^{w,\text{qll}} \sim \begin{cases} M_{A,0}^{8/3} (\hat{\lambda}_{\parallel}^w)^{1/3} \frac{v_{A,0}}{\ell_0} & M_{A,0}^4 \lesssim \hat{\lambda}_{\parallel}^w \lesssim M_{A,0} \\ M_{A,0}^{24/5} (\hat{\lambda}_{\parallel}^w)^{-1/5} \frac{v_{A,0}}{\ell_0} & \hat{\lambda}_{\parallel,*}^{w(\text{subA})} \lesssim \hat{\lambda}_{\parallel}^w \lesssim M_{A,0}^4 \\ M_{A,0}^4 (S_0 \hat{\lambda}_{\parallel}^w)^{1/2} \frac{v_{A,0}}{\ell_0} & \hat{\lambda}_{\parallel,\text{min}}^{w(\text{subA})} \lesssim \hat{\lambda}_{\parallel}^w \lesssim \hat{\lambda}_{\parallel,*}^{w(\text{subA})} \end{cases} \quad (14)$$

where $\hat{\lambda}_{\parallel,*}^{w(\text{subA})} \sim S_0^{1/5} (M_{A,0} \hat{\lambda}_{\perp,*}^{z(\text{subA})})^{8/5} \sim S_0^{-5/7} M_{A,0}^{8/7}$ is the wavelength below which the AW packet interacts with background fluctuations in the TMT regime, while $\hat{\lambda}_{\parallel,\text{min}}^{w(\text{subA})} \sim S_0^{1/5} (M_{A,0} \hat{\lambda}_{\perp,\text{min}}^{z(\text{subA})})^{8/5} \sim S_0^{-1}$ is the shortest wavelength at which the turbulent damping is effective.

The trans-Alfvénic regime is obtained from the above case, i.e., when there is no (WO) range:

[$M_{A,0} \approx 1$, with dynamic alignment]

$$\Gamma_{\text{transA}}^{w,\text{qll}} \sim \begin{cases} (\hat{\lambda}_{\parallel}^w)^{-1/5} \frac{v_{A,0}}{\ell_0} & S_0^{-5/7} \lesssim \hat{\lambda}_{\parallel}^w \lesssim 1 \\ (S_0 \hat{\lambda}_{\parallel}^w)^{1/2} \frac{v_{A,0}}{\ell_0} & S_0^{-1} \lesssim \hat{\lambda}_{\parallel}^w \lesssim S_0^{-5/7} \end{cases} \quad (15)$$

where we have explicitly written the transition and dissipation scales, i.e., $\hat{\lambda}_{\parallel,*}^{w(\text{transA})} \sim S_0^{1/5} (\hat{\lambda}_{\perp,*}^{z(\text{transA})})^{8/5} \sim S_0^{-5/7}$ and $\hat{\lambda}_{\parallel,\text{min}}^{w(\text{transA})} \sim S_0^{1/5} (\hat{\lambda}_{\perp,\text{min}}^{z(\text{transA})})^{8/5} \sim S_0^{-1}$, respectively.

One can see that when it comes to the interaction of the AW packet with anisotropic background fluctuations, including dynamic alignment in the picture changes the behaviour of the turbulent damping rate significantly with respect to the “classic” scenario (cf. Table 2). In the range of scales for which the packet interacts with critically balanced turbulence (i.e., $\lambda_{\parallel}^{w,\text{qll}} \lesssim \lambda_{\parallel,\text{CB}}^{w,\text{qll}}$), the damping rate due to this nonlinear interaction is always larger than the corresponding rate obtained without dynamic alignment (cf. equations (11)–(12) and Table 2; see also the left panel of Figure 1 for an immediate visual example). This can be understood by considering that dynamic alignment means a shallower perpendicular spectrum of background fluctuations ($-3/2$ instead of $-5/3$), and thus, at any scale $\lambda_{\perp}^z < \lambda_{\perp,\text{CB}}^z$, there is more turbulent power to nonlinearly damp the AW packet.

In general, if a CR-driven Alfvén-wave is injected in a background of sub-Alfvénic turbulence with dynamic alignment, now the damping rate interestingly exhibits two breaks that separate the three distinct regimes available in this scenario (contrary to the single break that would be present without dynamic alignment). This is a consequence of the new tearing-mediated regime that is only possible when a scale-dependent alignment takes place, and it is well summarized in Tables 1 and 2 (see also Appendix A). The first break is the same as in turbulence without dynamic alignment, and it occurs for wavelengths interacting with background fluctuations at the transition scale between weak and strong turbulence ($\lambda_{\parallel}^{w,\text{qll}} \sim \lambda_{\parallel,\text{CB}}^{w,\text{qll}} \sim M_{A,0}^4 \ell_0$). The second break instead emerges when the wavelength corresponds to a scale for which the AW packet starts to interact with tearing-mediated turbulence ($\lambda_{\parallel}^{w,\text{qll}} \sim \lambda_{\parallel,*}^{w(\text{subA})} \sim S_0^{-5/7} M_{A,0}^{8/7} \ell_0$). In astrophysical situations for which this damping mechanism is the main process that determines the efficiency of CR confinement, these breaks could leave a signature at the corresponding energies in the propagated spectrum of these cosmic particles (see Section 6 for a brief discussion about the values of $M_{A,0}$ and S_0 for which these breaks in the damping rate could be responsible of the features that are observed in the propagated CR spectrum).

4.2.2. super-Alfvénic turbulence ($M_{A,0} > 1$) with dynamic alignment

When background fluctuations are injected with $M_{A,0} > 1$ and dynamic alignment of critically balanced turbulent fluctuations takes place, an AW packet undergoes a turbulent damping with the following rate:

[$M_{A,0} > 1$, with dynamic alignment]

$$\Gamma_{\text{supA}}^{w,\text{qll}} \sim \begin{cases} M_{A,0} (\hat{\lambda}_{\parallel}^w)^{-2/3} \frac{v_{A,0}}{\ell_0} & M_{A,0}^{-3} \lesssim \hat{\lambda}_{\parallel}^w \lesssim 1 \\ M_{A,0}^{12/5} (\hat{\lambda}_{\parallel}^w)^{-1/5} \frac{v_{A,0}}{\ell_0} & \hat{\lambda}_{\parallel,*}^{w(\text{supA})} \lesssim \hat{\lambda}_{\parallel}^w \lesssim M_{A,0}^{-3} \\ M_{A,0}^3 (S_0 \hat{\lambda}_{\parallel}^w)^{1/2} \frac{v_{A,0}}{\ell_0} & \hat{\lambda}_{\parallel,\text{min}}^{w(\text{supA})} \lesssim \hat{\lambda}_{\parallel}^w \lesssim \hat{\lambda}_{\parallel,*}^{w(\text{supA})} \end{cases} \quad (16)$$

where $\hat{\lambda}_{\parallel,*}^{w(\text{supA})} \sim S_0^{1/5} M_{A,0}^{6/5} (\hat{\lambda}_{\perp,*}^{z(\text{supA})})^{8/5} \sim S_0^{-5/7} M_{A,0}^{-6/7}$ and the shortest wavelength for turbulent damping to be effective is $\hat{\lambda}_{\parallel,\text{min}}^{w(\text{supA})} \sim S_0^{1/5} M_{A,0}^{6/5} (\hat{\lambda}_{\perp,\text{min}}^{z(\text{supA})})^{8/5} \sim S_0^{-1}$.

Again, we stress that the isotropic normalized wavelength $\hat{\lambda}^w = \lambda^w/\ell_0$ enters the damping rate in the range $\ell_A \lesssim \lambda^w \lesssim \ell_0$,

Turbulent damping of quasi-parallel Alfvén waves with parallel wavelength λ_{\parallel}^w					
<i>background cascade</i> (acronym)	<i>scale range of interaction</i>		<i>scaling of the turbulent damping rate (Γ_{turb}^w):</i>		
	$\lambda_{\parallel,\text{max}}^w$	$\lambda_{\parallel,\text{min}}^w$	“FG04”	“L16”	<i>this work</i>
without scale-dependent alignment					
<i>sub-Alfvénic injection ($M_{A,0} < 1$):</i>					
(W0)	$M_{A,0} \ell_0$	$M_{A,0}^4 \ell_0$	—	$\omega_{A,0} M_{A,0}^{8/3} (\lambda_{\parallel}^w / \ell_0)^{-2/3}$	$\omega_{A,0} M_{A,0}^{8/3} (\lambda_{\parallel}^w / \ell_0)^{1/3}$
(GS95)	$M_{A,0}^4 \ell_0$	$S_0^{-1} \ell_0$	—	$\omega_{A,0} M_{A,0}^2 (\lambda_{\parallel}^w / \ell_0)^{-1/2}$	$\omega_{A,0} M_{A,0}^4$
<i>trans-Alfvénic injection ($M_{A,0} \approx 1$):</i>					
(GS95)	ℓ_0	$S_0^{-1} \ell_0$	$\omega_{A,0} (\lambda_{\parallel}^w / \ell_0)^{-1/2}$	—	$\omega_{A,0}$
<i>super-Alfvénic injection ($M_{A,0} > 1$):</i>					
(K41)	ℓ_0	$M_{A,0}^{-3} \ell_0$	—	$\omega_{A,0} M_{A,0} (\lambda_{\parallel}^w / \ell_0)^{-2/3}$	$\omega_{A,0} M_{A,0} (\lambda_{\parallel}^w / \ell_0)^{-2/3}$
(GS95)	$M_{A,0}^{-3} \ell_0$	$S_0^{-1} \ell_0$	—	$\omega_{A,0} M_{A,0}^{3/2} (\lambda_{\parallel}^w / \ell_0)^{-1/2}$	$\omega_{A,0} M_{A,0}^3$
with scale-dependent alignment					
<i>sub-Alfvénic injection ($M_{A,0} < 1$):</i>					
(W0)	$M_{A,0} \ell_0$	$M_{A,0}^4 \ell_0$	—	$\omega_{A,0} M_{A,0}^{8/3} (\lambda_{\parallel}^w / \ell_0)^{-2/3}$	$\omega_{A,0} M_{A,0}^{8/3} (\lambda_{\parallel}^w / \ell_0)^{1/3}$
(B06)	$M_{A,0}^4 \ell_0$	$M_{A,0}^{8/7} S_0^{-5/7} \ell_0$	—	—	$\omega_{A,0} M_{A,0}^{24/5} (\lambda_{\parallel}^w / \ell_0)^{-1/5}$
(TMT)	$M_{A,0}^{8/7} S_0^{-5/7} \ell_0$	$S_0^{-1} \ell_0$	—	—	$\omega_{A,0} M_{A,0}^4 S_0^{1/2} (\lambda_{\parallel}^w / \ell_0)^{1/2}$
<i>trans-Alfvénic injection ($M_{A,0} \approx 1$):</i>					
(B06)	ℓ_0	$S_0^{-5/7} \ell_0$	—	—	$\omega_{A,0} (\lambda_{\parallel}^w / \ell_0)^{-1/5}$
(TMT)	$S_0^{-5/7} \ell_0$	$S_0^{-1} \ell_0$	—	—	$\omega_{A,0} S_0^{1/2} (\lambda_{\parallel}^w / \ell_0)^{1/2}$
<i>super-Alfvénic injection ($M_{A,0} > 1$):</i>					
(K41)	ℓ_0	$M_{A,0}^{-3} \ell_0$	—	$\omega_{A,0} M_{A,0} (\lambda_{\parallel}^w / \ell_0)^{-2/3}$	$\omega_{A,0} M_{A,0} (\lambda_{\parallel}^w / \ell_0)^{-2/3}$
(B06)	$M_{A,0}^{-3} \ell_0$	$M_{A,0}^{-6/7} S_0^{-5/7} \ell_0$	—	—	$\omega_{A,0} M_{A,0}^{12/5} (\lambda_{\parallel}^w / \ell_0)^{-1/5}$
(TMT)	$M_{A,0}^{-6/7} S_0^{-5/7} \ell_0$	$S_0^{-1} \ell_0$	—	—	$\omega_{A,0} M_{A,0}^3 S_0^{1/2} (\lambda_{\parallel}^w / \ell_0)^{1/2}$

Table 2: Summary of the scaling relations for the turbulent damping rate Γ_{turb}^w of a quasi-parallel Alfvén wave in background MHD turbulence for the different regimes mentioned in Section 4. The damping rates obtained in this work are compared with the ones available in the existing literature, namely in Farmer and Goldreich (2004) (“FG04”) and in Lazarian (2016) (“L16”). The notation $\omega_{A,0} = v_{A,0} / \ell_0$ has been used. In all the regimes with dynamic alignment, a transition to a tearing-mediated range (TMT) has been assumed, i.e., that $S_0 \gg M_{A,0}^{-4}$ ($S_0 \gg M_{A,0}^3$) holds for sub-Alfvénic (super-Alfvénic) injection.

i.e., where the AW packet interacts with hydrodynamic-like pre-existing turbulence. In this range of scales, the result is unchanged with respect to the turbulent damping rate obtained without dynamic alignment (Section 4.1.2). At smaller scales $\lambda_{\parallel}^{w,\text{qll}} \lesssim \ell_A$, the quasi-parallel condition in (6) applies again and the damping rate depends explicitly on the normalized parallel wavelength $\lambda_{\parallel}^w = \lambda_{\parallel}^{w,\text{qll}} / \ell_0$. In this regime, the turbulent

damping rate differs significantly from the one obtained without dynamic alignment. When a scale-dependent alignment of fluctuations is taken into account, the turbulent damping is always much more effective than in the case obtained without dynamic alignment. This leads to a damping rate that can be larger by orders of magnitude with respect to the one in (13), depending on the Alfvénic Mach number $M_{A,0}$ and on the Lun-

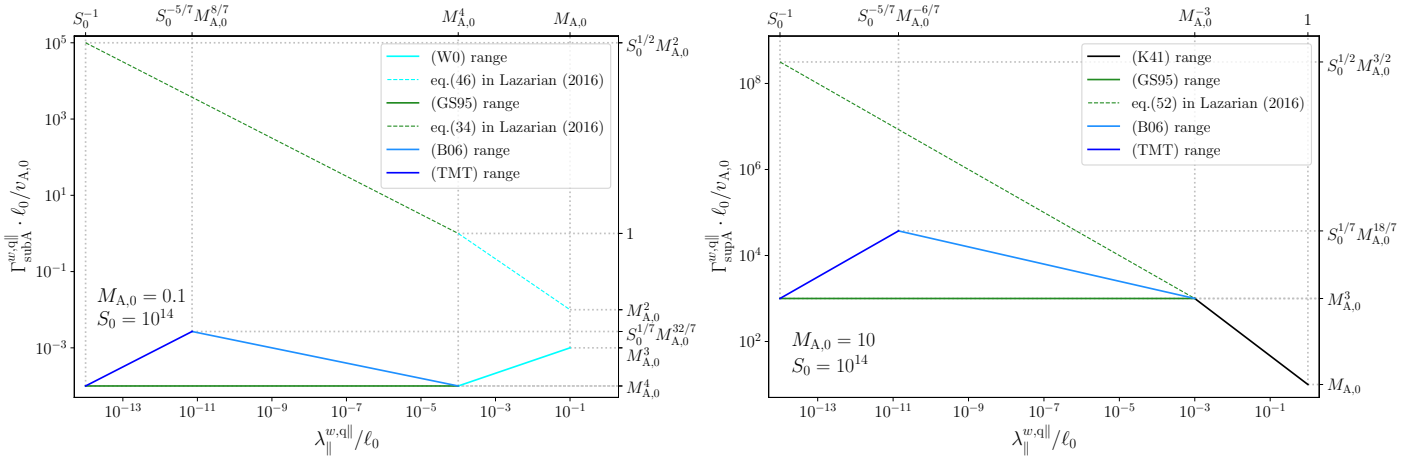


Fig. 1: Normalized turbulent damping rate $\frac{\ell_0}{v_{A,0}} \Gamma_{\text{turb}}^{w,q||}$ for quasi-parallel AW packets with normalized parallel wavelength $\lambda_{||}^{w,q||} / \ell_0$, in a background plasma with Lunquist number $S_0 = 10^{14}$ and different turbulent regimes (see Appendix A). Solid lines represent damping rates derived in this work (equations (11), (13), (14), and (16)), while dashed lines report the damping rates in Lazarian (2016) for reference. General expressions for transition scales and damping-rate values are reported on the right and upper axis. Left: damping rates in sub-Alfvénic turbulence ($M_{A,0} = 0.1$). Right: damping rates in super-Alfvénic turbulence ($M_{A,0} = 10$).

quist number S_0 at injection scales (see Table 2 for a comparison of the scaling and the right panel of Figure 1 for an explicit graphic example). Finally, analogously to the case with $M_{A,0} < 1$, the damping rate exhibits two breaks also in a background of super-Alfvénic turbulence, if dynamic alignment can occur. The first break emerges for wavelengths comparable to the transition scale between hydrodynamic-like and critically balanced turbulence ($\lambda^w \sim \ell_A \sim M_{A,0}^{-3} \ell_0$). A second break occurs at wavelengths corresponding to the scale marking the transition between a dynamically aligned cascade and the tearing-mediated range ($\lambda_{||}^{w,q||} \sim \lambda_{||,*}^w \sim S_0^{-5/7} M_{A,0}^{-6/7} \ell_0$). For which values of $M_{A,0}$ and S_0 these breaks in the damping rate could be responsible of the features that are observed in the propagated CR spectrum is briefly discussed in Section 6.

5. Feedback on background fluctuations

When deriving the scaling of $\Gamma_{\text{turb}}^{w,q||}$ in the previous Section, we have neglected the feedback that the injected Alfvén-wave packets could have on pre-existing turbulent fluctuations. In general, background fluctuations could also be affected by their nonlinear interaction with these AW packets—let us call it “feedback”. It is therefore instructive to understand when such effect has to be taken into account. The relevance of this feedback can be estimated by comparing two timescales:

1. The intrinsic cascade time of background fluctuations, i.e., the timescale of the cascade process induced by pre-existing (counter-propagating) fluctuations on themselves, $\tau_{\text{casc}}^{(z|z)} \sim \tau_{\text{nl}}^{(z|z)} / \chi^{(z|z)}$ (or just $\tau_{\text{casc}}^{(z|z)} \sim \tau_{\text{nl}}^{(z|z)}$, if $\chi^{(z|z)} \gtrsim 1$).
2. The CR-induced cascade time, i.e., the timescale of the cascade that would be induced by the injected AW packets on the background fluctuations, $\tau_{\text{casc}}^{(z|w)} \sim \tau_{\text{nl}}^{(z|w)} / \chi^{(z|w)}$ (or just $\tau_{\text{casc}}^{(z|w)} \sim \tau_{\text{nl}}^{(z|w)}$, if $\chi^{(z|w)} \gtrsim 1$).

Hereafter, the simpler super-script “z” will be used instead of “(z|z)” for the sake of homogeneity of notation with the previous Sections. Moreover, for the sake of clarity in the qualitative discussion that will follow, the effect of dynamic alignment will

not be taken into account in this Section. The nonlinear parameter $\chi^{(z|w)}$ describing the interaction of background fluctuations with CR-driven AW packets is $\chi_{\lambda_{\perp}}^{(z|w)} \sim (\lambda_{||,\lambda_{\perp}}^z / \lambda_{\perp}^z) (\delta w_{\lambda_{\perp}} / v_{A,0}) \sim (\delta w_{\lambda_{\perp}} / \delta z_{\lambda_{\perp}}) \chi_{\lambda_{\perp}}^z$, while the timescale associated to such nonlinear interaction is $\tau_{\text{nl},\lambda_{\perp}}^{(z|w)} \sim \lambda_{\perp} / \delta w_{\lambda_{\perp}} \sim (\delta z_{\lambda_{\perp}} / \delta w_{\lambda_{\perp}}) \tau_{\text{nl},\lambda_{\perp}}^z$. The ratio of the two cascade timescales is thus given by:

$$\frac{\tau_{\text{casc}}^{(z|w)}}{\tau_{\text{casc}}^{(z|z)}} \sim \begin{cases} (\delta z_{\lambda_{\perp}} / \delta w_{\lambda_{\perp}})^2 & \text{if } \begin{cases} \chi_{\lambda_{\perp}}^z < 1 \text{ and } \chi_{\lambda_{\perp}}^{(z|w)} \lesssim 1 \\ \text{or} \\ \chi_{\lambda_{\perp}}^z \sim 1 \text{ and } \chi_{\lambda_{\perp}}^{(z|w)} < 1 \end{cases} \\ (\delta z_{\lambda_{\perp}} / \delta w_{\lambda_{\perp}}) \chi_{\lambda_{\perp}}^z & \text{if } \chi_{\lambda_{\perp}}^z < 1 \text{ and } \chi_{\lambda_{\perp}}^{(z|w)} > 1 \\ (\delta z_{\lambda_{\perp}} / \delta w_{\lambda_{\perp}}) & \text{if } \chi_{\lambda_{\perp}}^z \sim 1 \text{ and } \chi_{\lambda_{\perp}}^{(z|w)} \gtrsim 1 \\ (\delta z_{\lambda} / \delta w_{\lambda}) (\delta w_{\lambda} / v_{A,0})^{-1} & \text{if } \chi_{\lambda}^z > 1 \text{ and } \chi_{\lambda}^{(z|w)} < 1 \\ (\delta z_{\lambda} / \delta w_{\lambda}) & \text{if } \chi_{\lambda}^z > 1 \text{ and } \chi_{\lambda}^{(z|w)} \gtrsim 1 \end{cases} \quad (17)$$

Feedback effects shall be taken into account if the nonlinear cascade process that would be induced by the injected Alfvén-wave packets becomes faster than the intrinsic cascading process of background fluctuations, i.e., at scales where $\tau_{\text{casc}}^{(z|w)} / \tau_{\text{casc}}^{(z|z)} \lesssim 1$. From (17) one can see that “cosmic-ray feedback” (CRF) is relevant at scales for which self-generated waves achieve non-negligible amplitudes with respect to the background fluctuations. Clearly, the weaker the damping, the larger the amplitude that self-generated fluctuations can attain. Hence, feedback on background turbulence becomes more important as the most-relevant damping mechanism becomes weaker; and this is a general statement that does not depend on which damping process determines the saturation level of CR-generated waves. The scales at which CRF has to be taken into account thus requires to compare the scale-dependent amplitudes of both the CR-driven AW packets (δw_{λ}) and the pre-existing background fluctuations (δz_{λ}). A precise estimate of these scales requires a detailed knowledge of how the CRSI saturation level in pre-

existing turbulence depends upon plasma parameters and background conditions, which is not yet achieved. At this stage, we provide only a general, qualitative discussion.

Let us consider cases in which the CRSI saturates at a level $(\delta w/v_{A,0})^2 \sim (\delta B^{(\text{CRSI})}/B_0)^2 \ll 1$. Then, from (17) one can see that when the CR-driven AW packets interact with super-Alfvénic turbulence ($M_{A,0} > 1$), and at scales where the cascade is hydrodynamic-like ($\lambda^w \gtrsim \ell_A$), the ratio $\tau_{\text{casc}}^{(z|w)}/\tau_{\text{casc}}^z$ is typically much larger than unity. Therefore, when the CR-driven instability produces fluctuations at a level $\delta B^{(\text{CRSI})}/B_0 \ll 1$ (which depends also on the presence of a mean field B_0), cosmic-ray feedback is likely negligible at all scales belonging to the (K41) regime. The situation is different for trans- and sub-Alfvénic injection ($M_{A,0} \lesssim 1$), or for super-Alfvénic injection at scales below which the hydrodynamic-like cascade transitions to the critically balanced regime ($\lambda_{\parallel}^w < \ell_A$). In these cases, the CR feedback on pre-existing turbulence is negligible only at scales for which the packets' amplitudes are smaller than the background fluctuations' level. As a consequence, cosmic-ray feedback should be taken into account at scales $\lambda_{\perp} \lesssim \lambda_{\perp}^{\text{CRF}}$, where the (perpendicular) CR-feedback scale $\lambda_{\perp}^{\text{CRF}}$ is defined as the scale at which $\delta w_{\lambda_{\perp}^{\text{CRF}}} \sim \delta z_{\lambda_{\perp}^{\text{CRF}}}$ holds. If $\delta B^{(\text{CRSI})}/B_0$ is sufficiently small, such scale may be smaller than the turbulent dissipation scale, and thus the feedback could be neglected for all purposes of CR transport. However, the growth and saturation level of the CRSI depends upon the CR-to-thermal density ratio $n_{\text{CR}}/n_{\text{th}}$. In the Galactic halo this ratio is negligibly small, and the above reasoning likely applies. This may not be the case near CR sources, where such density ratio is not so small and CRs can further evacuate the thermal gas (Schroer et al. 2021, 2022). We thus expect this feedback to be relevant in these environments. This issue will be addressed in more detail and quantitatively in the accompanying Paper II.

Finally, we remark that the discussion above regarding the scale at which the CR feedback could become relevant was done in terms of perpendicular scales λ_{\perp} (see equation (17)). This means that we denoted with $\lambda_{\perp}^{\text{CRF}}$ the perpendicular scale at which CR-generated waves affects pre-existing turbulence. However, regardless of the damping mechanism that saturates the amplitude of the fluctuations, the CRSI growth rate is such that quasi-parallel Alfvén waves $\lambda_{\parallel}^w \ll \lambda_{\perp}^w$ are mainly produced. It is thus convenient to relate the scale $\lambda_{\perp}^{\text{CRF}}$ at which the CR-driven fluctuations' amplitude becomes comparable to the amplitude of background fluctuations to the injected parallel wavelength $\lambda_{\parallel}^{w,\text{qll}}$. This can be done by using the quasi-parallel condition (6), i.e.,

$$\lambda_{\parallel}^{\text{CRF}} \sim \left(\frac{\delta z_{\lambda_{\perp}^{\text{qll}}}}{v_{A,0}} \right) \lambda_{\perp}^{\text{CRF}} \ll \lambda_{\perp}^{\text{CRF}}. \quad (18)$$

Hence, a quasi-parallel Alfvén waves $\delta w_{\lambda_{\parallel}}$ driven by CRs at scales $\lambda_{\parallel}^{w,\text{qll}} \lesssim \lambda_{\parallel}^{\text{CRF}}$ can actually affect pre-existing turbulent fluctuations $\delta z_{\lambda_{\perp}}$ on much larger scales $\lambda_{\perp}^{\text{CRF}} \gtrsim \lambda_{\perp} \gg \lambda_{\parallel}^{w,\text{qll}}$. (We recall that we assume that nonlinear interactions are local in perpendicular scale, so in what follows we do not need to distinguish between the two scales λ_{\perp}^w and λ_{\perp}^z , i.e., $\lambda_{\perp}^w \sim \lambda_{\perp}^z \sim \lambda_{\perp}$).

In the following, we attempt to provide two phenomenological models for the CR-modified cascade of background fluctuations. However, these are just plausible models at this stage. Focused numerical investigations will be necessary in order to verify if (and under which circumstances) they can be realized.

5.1. A phenomenological model for CR-modified scaling of pre-existing turbulent fluctuations

A simple phenomenological model for the cascade modified by the CR-generated AW packets can be constructed as follows.

Let assume that, at scales where $\chi_{\lambda_{\perp}}^z \lesssim 1$, pre-existing fluctuations and their anisotropy follow the scaling $\delta z_{\lambda_{\perp}}^{(0)} \propto \lambda_{\perp}^{\alpha_{\perp}^z}$ and $\lambda_{\parallel,\lambda_{\perp}} \propto \lambda_{\perp}^{\alpha_{\perp}^z}$, respectively, with $\alpha_{\perp}^z > 0$. For critically balanced fluctuations ($\chi^z \sim 1$) the anisotropy is such that $\delta^z = 1 - \alpha_{\perp}^z$, while in weak turbulence ($\chi^z < 1$) it is $\delta^z = 0$. Such scaling for the fluctuations corresponds to a perpendicular power spectrum $E_{\delta z}^{(0)}(k_{\perp}) \propto k_{\perp}^{-\xi_{\perp}^z}$, with $\xi_{\perp}^z = 1 + 2\alpha_{\perp}^z$. At scales where $\chi_{\lambda_{\perp}}^z > 1$, the scaling is isotropic (i.e., $\delta^z = 1$), and so $\delta z_{\lambda_{\perp}}^{(0)} \propto \lambda_{\perp}^{\alpha^z}$ and $E_{\delta z}^{(0)}(k) \propto k^{-\xi^z}$, with $\xi^z = 1 + 2\alpha^z$. These are the ‘‘unperturbed’’ properties of background fluctuations, i.e., without CR feedback, and are thus denoted by a ‘‘(0)’’ superscript. Then let assume a scaling $\delta w_{\lambda_{\parallel}} \propto (\lambda_{\parallel}^w)^{-\alpha_{\parallel}^w}$ for the CR-driven (quasi-parallel) fluctuations, corresponding to a parallel power spectrum $E_{\text{CRSI}}(k_{\parallel}^w) \propto (k_{\parallel}^w)^{\xi_{\parallel}^w}$, where $\xi_{\parallel}^w = 2\alpha_{\parallel}^w - 1$. At scales λ_{\perp} where background fluctuations are sub-Alfvénic and anisotropic (i.e., such that $\chi_{\lambda_{\perp}}^z \lesssim 1$), the quasi-parallel condition (6) holds for CR-driven waves. Hence, the corresponding perpendicular scaling for self-generated fluctuations is typically steeper than its parallel counterpart, and is related to the perpendicular scaling of pre-existing fluctuations, namely $\delta w_{\lambda_{\perp}} \propto \lambda_{\perp}^{-\alpha_{\perp}^w}$ with $\alpha_{\perp}^w = \alpha_{\parallel}^w (1 + \alpha_{\perp}^z)$. This corresponds to a perpendicular spectrum $E_{\text{CRSI}}(k_{\perp}) \propto (k_{\perp})^{\xi_{\perp}^w}$, with $\xi_{\perp}^w = 2\alpha_{\parallel}^w (1 + \alpha_{\perp}^z) - 1 = \xi_{\parallel}^w + (\xi_{\parallel}^w + 1)(\xi_{\perp}^z - 1)/2$. On the other hand, at scales where $\chi_{\lambda_{\perp}}^z > 1$, the distinction between α_{\perp}^w and α_{\parallel}^w is lost. In this case, we just assume a scaling $\delta w_{\lambda} \propto \lambda^{-\alpha^w}$ and a (isotropic) power spectrum $E_{\text{CRSI}}(k) \propto (k)^{\xi^w}$ with $\xi^w = 2\alpha^w - 1$.

Before proceeding further, it is worth mentioning that here we are considering a generic case where self-generated turbulence can be described by a power-law spectrum, without making any assumption on its spectral index nor on the damping mechanism that sets the saturation of the instability. The only condition that we will require is that the hierarchy of possible interactions between CR-generated waves and pre-existing turbulent fluctuations is self consistent, i.e., that background turbulence is affected by the self-generated waves before turbulence can affect the waves. In this regard, one can verify that when $\tau_{\text{casc}}^{(z|w)} \ll \tau_{\text{casc}}^z$ holds, then the condition $\tau_{\text{casc}}^{(z|w)} \ll \tau_{\text{casc}}^w \sim (\Gamma_{\text{turb}}^{w,\text{qll}})^{-1}$ is automatically satisfied:⁷ this condition allows to neglect a mutual feedback between background fluctuations and CR-driven Alfvén waves, i.e., to consider only the modification to the scaling of pre-existing turbulence induced by a stationary spectrum of (saturated) self-generated fluctuations.

We now want to know how the scaling of $\delta z^{(0)}$ are modified by the presence of δw , knowing that we are in a regime in which such feedback is faster than the intrinsic cascade time of $\delta z^{(0)}$ (viz., $\tau_{\text{casc}}^{(z|w)} \ll \tau_{\text{casc}}^z$). Within these assumptions, we can derive the scaling of CR-modified turbulence by replacing the cascade

⁶ The quasi-parallel condition, i.e., $k_{\parallel}^w \sim (\delta z_{k_{\perp}}/v_{A,0})^{-1} k_{\perp}$, and condition on the total energy, i.e., $(k_{\parallel}^w)^{-1} (\delta w_{k_{\parallel}^w})^2 dk_{\parallel}^w \sim k_{\perp}^{-1} (\delta w_{k_{\perp}})^2 dk_{\perp}$, have been employed to derive the perpendicular scaling of the fluctuations, $\delta w_{k_{\perp}}$.

⁷ To show this, one multiplies by $\Gamma_{\text{turb}}^{w,\text{qll}}$ both sides of the condition $\tau_{\text{casc}}^{(z|w)} \ll \tau_{\text{casc}}^z$ and obtain the equivalent condition $\Gamma_{\text{turb}}^{w,\text{qll}} \tau_{\text{casc}}^{(z|w)} \ll \Gamma_{\text{turb}}^{w,\text{qll}} \tau_{\text{casc}}^z$. Then, using (9)-(10), one can show that $\Gamma_{\text{turb}}^{w,\text{qll}} \tau_{\text{casc}}^z \lesssim 1$ holds for any value of χ^w and χ^z , which further implies the condition $\Gamma_{\text{turb}}^{w,\text{qll}} \tau_{\text{casc}}^{(z|w)} \ll 1$.

timescale,

$$\tau_{\text{casc}}^z \rightarrow \tau_{\text{casc}}^{(z|w)}, \quad (19)$$

by rescaling the unperturbed background fluctuations into a “1st-order modified” fluctuations (denoted by a “(1)” superscript),

$$\delta z_{\lambda_{\perp}}^{(0)} \rightarrow \delta z_{\lambda_{\perp}}^{(1)} = \zeta_{\lambda_{\perp}} \delta z_{\lambda_{\perp}}^{(0)}, \quad (20)$$

and by requiring that the cascade rate is still scale-independent, i.e., $(\delta z_{\lambda_{\perp}}^{(1)})^2 / \tau_{\text{casc}}^{(z|w)} \sim \varepsilon \sim \text{const}$. This procedure readily provides the scaling factor

$$\zeta_{\lambda_{\perp}} \sim \left(\frac{\tau_{\text{casc}}^{(z|w)}}{\tau_{\text{casc}}^z} \right)^{1/2}, \quad (21)$$

which can be estimated using (17) for the various χ^z and χ^w regimes, and, as a first approximation, by employing the unperturbed scaling $\delta z_{\lambda_{\perp}}^{(0)}$; the rescaling factor computed in this way will be denoted as $\zeta_{\lambda_{\perp}}^{(0)}$.⁸ The resulting CR-modified perpendicular power spectrum of background fluctuations is then given by $E_{\delta z}^{(1)}(k_{\perp}) \sim (\zeta_{\lambda_{\perp}}^{(0)})^2 E_{\delta z}^{(0)}(k_{\perp})$, i.e., $E_{\delta z}^{(1)}(k_{\perp}) \propto k_{\perp}^{-(\xi_{\perp}^z + \Delta \xi_{\perp}^{\text{CRF}})}$, where the CR-induced modification of the spectral index is

$$\Delta \xi_{\perp}^{\text{CRF}} \sim \begin{cases} \frac{1}{2}(\xi_{\perp}^z + 1)(\xi_{\parallel}^w + 3) - 2 & \text{if } \left\{ \begin{array}{l} \chi_{\lambda_{\perp}}^z < 1 \text{ and } \chi_{\lambda_{\perp}}^{(z|w)} \lesssim 1 \\ \text{or} \\ \chi_{\lambda_{\perp}}^z \sim 1 \text{ and } \chi_{\lambda_{\perp}}^{(z|w)} < 1 \end{array} \right. \\ \frac{1}{4}(\xi_{\perp}^z + 1)(\xi_{\parallel}^w + 5) - 3 & \text{if } \chi_{\lambda_{\perp}}^z < 1 \text{ and } \chi_{\lambda_{\perp}}^{(z|w)} > 1 \\ \frac{1}{4}(\xi_{\perp}^z + 1)(\xi_{\parallel}^w + 3) - 1 & \text{if } \chi_{\lambda_{\perp}}^z \sim 1 \text{ and } \chi_{\lambda_{\perp}}^{(z|w)} \gtrsim 1 \\ \frac{1}{2}(\xi_{\perp}^z + 2\xi_{\parallel}^w + 1) & \text{if } \chi_{\lambda_{\perp}}^z > 1 \text{ and } \chi_{\lambda_{\perp}}^{(z|w)} < 1 \\ \frac{1}{2}(\xi_{\perp}^z + \xi_{\parallel}^w) & \text{if } \chi_{\lambda_{\perp}}^z > 1 \text{ and } \chi_{\lambda_{\perp}}^{(z|w)} \gtrsim 1 \end{cases} \quad (22)$$

We remind that this result is only valid at scales where $\zeta_{\lambda_{\perp}} < 1$, and only if $\Gamma_{\text{turb}}^{w, \text{qll}} \tau_{\text{casc}}^{(z|w)} \ll 1$ (i.e., if the CR-driven Alfvén-wave packets are unaffected by pre-existing fluctuations). It is interesting to note that the anisotropy of the pre-existing cascade would be unaffected if $\chi_{\lambda_{\perp}}^{(z|w)} < 1$ (leaving $\ell_{\parallel, \lambda_{\perp}} \approx \text{const}$. if $\chi^z < 1$, or $\ell_{\parallel, \lambda_{\perp}} \propto \lambda_{\perp}^{\xi_{\perp}^z}$ if $\chi^z \sim 1$), or if $\chi^z > 1$ (leaving $\ell_{\parallel, \lambda_{\perp}} \propto \lambda_{\perp}$). On the other hand, if $\chi_{\lambda_{\perp}}^{(z|w)} \sim 1$, a critical balance between the Alfvén time τ_A^z and the nonlinear time $\tau_{\text{nl}}^{(z|w)}$ would be established, leading to a modified anisotropy $\ell_{\parallel, \lambda_{\perp}} \propto \lambda_{\perp}^{1+\alpha_{\perp}^w} = \lambda_{\perp}^{\delta^z + \delta^{\text{CRF}}}$ with $\delta^{\text{CRF}} = \alpha_{\parallel}^w + \alpha_{\perp}^z (\alpha_{\parallel}^w - 1)$. This means that the anisotropy of pre-existing fluctuations would be reduced if $|\alpha_{\parallel}^w| < \alpha_{\perp}^z / (1 + \alpha_{\perp}^z)$

⁸ One can imagine to perform an expansion of the rescaling factor based on iteratively modified timescales $\tau_{\text{casc}, \lambda_{\perp}}^{(n)}$, and rewrite it as a series $\zeta_{\lambda_{\perp}} = (\tau_{\text{casc}, \lambda_{\perp}}^{(z|w)})^{1/2} \left(\sum_n 1/\tau_{\text{casc}, \lambda_{\perp}}^{(n)} \right)^{1/2} = \zeta_{\lambda_{\perp}}^{(0)} \left(1 + \sum_{n>0} \tau_{\text{casc}, \lambda_{\perp}}^{(0)} / \tau_{\text{casc}, \lambda_{\perp}}^{(n)} \right)^{1/2}$ (recall that we have assumed that the CR-driven fluctuations $\delta w_{\lambda_{\perp}}$ are unaffected by background fluctuations). The ratio of 0th to n th timescale is $\tau_{\text{casc}, \lambda_{\perp}}^{(0)} / \tau_{\text{casc}, \lambda_{\perp}}^{(n)} \propto \delta z_{\lambda_{\perp}}^{(n)} / \delta z_{\lambda_{\perp}}^{(0)}$ (or even $\propto (\delta z_{\lambda_{\perp}}^{(n)} / \delta z_{\lambda_{\perp}}^{(0)})^2$). Then, if the CR-induced modification of the pre-existing spectrum is a steepening, the cascade timescale would significantly increase at increasing n , i.e., $\tau_{\text{casc}, \lambda_{\perp}}^{(n)} \gg \tau_{\text{casc}, \lambda_{\perp}}^{(n-1)} \gg \dots \gg \tau_{\text{casc}, \lambda_{\perp}}^{(1)} \gg \tau_{\text{casc}, \lambda_{\perp}}^{(0)}$. So, if the series converges and its contribution is negligible (which shall be verified), $\zeta_{\lambda_{\perp}} \approx \zeta_{\lambda_{\perp}}^{(0)}$.

(e.g., for GS95 turbulence, this means $|\alpha_{\parallel}^w| < 1/4$, corresponding to a CR-driven spectrum $\propto k_{\parallel}^{-1/2}$ or steeper), and it would be instead increased otherwise.

As mentioned before, the exact scaling and amplitude of the self-generated turbulent spectrum depends both on the properties of the CR distribution that drives the instability and on the different damping mechanisms that contribute to the instability saturation (see, e.g., [Marcowith et al. 2021](#), and references therein). However, as an example, let us consider the results obtained with 1D-3V kinetic simulations in [Holcomb and Spitkovsky \(2019\)](#), where the CR-driven fluctuations at saturation developed a scaling roughly consistent with $\delta B \propto k_{\parallel}^{-1/2}$ (i.e., $\alpha_{\parallel}^w \approx -1/2$ and thus $\xi_{\parallel}^w \approx -2$). Assuming a GS95 cascade of the background fluctuations (i.e., $\chi^z \sim 1$ and $\xi_{\perp}^z = 5/3$) and strong nonlinearities induced by the CR-driven waves on these fluctuations (i.e., $\chi_{\lambda}^{(z|w)} \gtrsim 1$), one obtains $\Delta \xi_{\perp}^{\text{CRF}} \approx 1/3$. This means that the spectrum of background fluctuations below $\lambda_{\perp}^{\text{CRF}}$ would be steepened from $k_{\perp}^{-5/3}$ to k_{\perp}^{-2} due to the CR feedback (and also further suppressing the turbulent damping by lowering the amplitude of background fluctuations at those scales; cf. equation (10)). The anisotropy of background turbulence would be also significantly increased, from $k_{\parallel} \propto k_{\perp}^{2/3}$ to $k_{\parallel} \propto k_{\perp}^{-1/3}$ (thus further reducing the effectiveness of CR scattering on pre-existing fluctuations). Another example can be set by assuming an Iroshnikov-Kraichnan spectrum for self-generated turbulence ($\propto k^{-3/2}$). In fact, this type of spectrum has been often invoked to explain the observed γ -ray emission and local CR data (e.g., [Gaggero et al. 2015](#), and references therein). In this case, still assuming a GS95-type of background turbulence and $\chi_{\lambda}^{(z|w)} \gtrsim 1$, one now obtains that the background spectrum is unchanged ($\Delta \xi_{\perp}^{\text{CRF}} \approx 0$) but the anisotropy is enhanced by the CR feedback ($k_{\parallel} \approx \text{const}$).

5.1.1. Over-critical interaction ($\chi_{\lambda}^{(z|w)} > 1$) and alternative CR-modified scaling of pre-existing fluctuations

When nonlinear interactions between the CR-driven Alfvén-wave packets and background turbulence are “over-critical”, i.e., $\chi_{\lambda}^{(z|w)} > 1$, it is reasonable to consider that pre-existing scaling are not just perturbatively modified. Therefore, we present an alternative model in which the intrinsic cascade time of pre-existing fluctuations τ_{casc}^z is completely replaced by the nonlinear timescale $\tau_{\text{nl}}^{(z|w)}$, without further re-scaling of $\delta z^{(0)}$ as in (21). This allows to directly derive the CR-modified scaling of background fluctuations δz^{CRF} by requiring $(\delta z^{\text{CRF}})^2 / \tau_{\text{nl}}^{(z|w)} \sim \varepsilon = \text{const}$.

If $\chi^z \lesssim 1$, pre-existing scaling are anisotropic, and the condition above yields the perpendicular scaling

$$\frac{\delta w_{\lambda_{\perp}} (\delta z_{\lambda_{\perp}}^{\text{CRF}})^2}{\lambda_{\perp}} \sim \varepsilon = \text{const.} \Rightarrow \delta z_{\lambda_{\perp}}^{\text{CRF}} \propto \lambda_{\perp}^{(1+\alpha_{\perp}^w)/2}. \quad (23)$$

This corresponds to a modified perpendicular spectrum $E_{\delta z}^{\text{CRF}}(k_{\perp}) \propto k_{\perp}^{-(\xi_{\perp}^z + \Delta \xi_{\perp}^{\text{CRF}})}$ with

$$\Delta \xi_{\perp}^{\text{CRF}} = \frac{\xi_{\parallel}^w + \xi_{\perp}^z (\xi_{\parallel}^w - 3) + 9}{4}, \quad (24)$$

where the link to the the original scaling of pre-existing fluctuations is a consequence of the quasi-parallel condition (6).

If $\chi^z > 1$, CR-modified fluctuations would follow the isotropic scaling $\delta z_{\lambda}^{\text{CRF}} \propto \lambda^{(1+\alpha_{\perp}^w)/2}$, corresponding to a spectrum

$$E_{\delta z}^{\text{CRF}}(k) \propto k^{-(\xi^w + 5)/2}, \quad (25)$$

which does not depend on the original scaling of pre-existing fluctuations due to the loss of “quasi-parallel” concept.

6. Discussion and conclusions

The turbulent damping of an Alfvén-wave (AW) packet excited by cosmic-rays (CRs) in pre-existing incompressible magnetohydrodynamic (MHD) turbulence is re-examined by carefully taking into account the role of the “nonlinearity parameter” χ^w that quantifies the strength of the nonlinear interaction between the packet and background fluctuations. In particular, the difference between χ^w and the nonlinear parameter χ^z that instead describes the regime of background turbulence (i.e., the intrinsic strength of nonlinear interactions between pre-existing fluctuations) has been elucidated. The derivation of turbulent damping rates in a “classic” MHD turbulence scenario (i.e., without the so-called “dynamic alignment”) has thus been revised taking into account such difference between χ^w and χ^z , and new scaling relations for the damping rates have been obtained. Furthermore, by considering most-recent theories of MHD turbulence that account for a scale-dependent (“dynamic”) alignment of fluctuations and the possibility of a reconnection-mediated regime, completely new damping rates have been also obtained for the first time. Finally, the role of cosmic-ray feedback (CRF) on pre-existing turbulence is also examined and a simple criterion for CRF effects is derived. Two very simple phenomenological models of CR-modified scaling of background fluctuations are also obtained. In particular, this feedback can steepen the spectrum of background turbulence and further enhance its spectral anisotropy ($k_{\parallel} \ll k_{\perp}$). By reducing the amplitude of pre-existing fluctuations at the CRF scales, the former effect would have the consequence of further reducing the turbulent damping rate at those scales. At the same time, the increased anisotropy of background turbulence would also reduce the effectiveness of CR resonant scattering on pre-existing fluctuations at the CRF scales. These two CR-feedback effects may thus clear the stage for self-generated turbulence to dominate the CR transport and reinforce the self-confinement picture. Taking into account the feedback of CR-generated fluctuations on pre-existing turbulence may be relevant in astrophysical environments where the density of cosmic-ray n_{CR} is not negligible with respect to the density of the background thermal plasma n_{th} (e.g., near CR sources). The issue of CRF effects, as well as the role of other damping mechanisms, will be addressed in more detail in the following Paper II.

The main features of the new turbulent damping rates obtained in this work can be summarized as follows:

- The nonlinear interaction between a quasi-parallel (q||) AW packet and pre-existing anisotropic turbulence is always weak (equations (7)-(8)). As a result, the turbulent damping rate of the packets depends on the background-fluctuations’ amplitude to the third power (equation (10)), and thus is strongly suppressed with respect to what previously estimated. This is true at any wavelength when the AW packet interacts with sub- and trans-Alfvénic turbulence, and also for those packets whose wavelength interacts with fluctuations at scales where they become critically balanced in the case of super-Alfvénic injection.
- How the turbulent damping rate $\Gamma_{\text{turb}}^{w,q||}$ depends on (i) the AW-packet’s parallel wavelength λ_{\parallel} (and thus on the CR gyro-radius from which it is excited) and on (ii) the injection-scale Alfvénic Mach number $M_{A,0}$, in the “classic”

MHD turbulence scenario is significantly different from what is present in the existing literature (equations (11)-(13)). In fact, the damping rate agrees with the literature only when the AW packet interacts with isotropic (“K41”) turbulence, namely $\Gamma_{\text{K41}}^w \propto M_{A,0} \lambda^{-2/3}$. On the contrary, when the packet interacts with weak turbulence (“W0”), the damping rate scales as $\Gamma_{\text{W0}}^{w,q||} \propto M_{A,0}^{8/3} \lambda_{\parallel}^{1/3}$ (instead of $\propto M_{A,0}^{8/3} \lambda_{\parallel}^{-2/3}$ previously obtained), while when it interacts with critically balanced turbulence (“GS95”), turbulent damping does not depend on the wavelength, i.e., $\Gamma_{\text{GS95}}^{w,q||} \sim \text{const.}$ (and it is $\propto M_{A,0}^4$ for $M_{A,0} < 1$ or $\propto M_{A,0}^3$ if $M_{A,0} > 1$, instead of $\propto M_{A,0}^2 \lambda_{\parallel}^{-1/2}$ or $\propto M_{A,0} \lambda_{\parallel}^{-1/2}$, respectively, as reported in existing literature).

- Including dynamic alignment of pre-existing fluctuations in the picture, and thus allowing also for the possibility of a reconnection-mediated range, introduces novel regimes and breaks in the turbulent damping rate (equations (14)-(16)). When a quasi-parallel AW packet interacts with critically balanced and dynamically aligning anisotropic turbulence (“B06”), it is subject to a damping rate $\Gamma_{\text{B06}}^{w,q||} \propto M_{A,0}^{24/5} \lambda_{\parallel}^{-1/5}$ if $M_{A,0} < 1$ or $\Gamma_{\text{B06}}^{w,q||} \propto M_{A,0}^{12/5} \lambda_{\parallel}^{-1/5}$ if $M_{A,0} > 1$. Alfvén-wave packets that interact with tearing-mediated turbulence (“TMT”) are instead subject to a damping rate that is now sensitive also to the injection-scale Lundquist number S_0 , and it scales as $\Gamma_{\text{TMT}}^{w,q||} \propto M_{A,0}^4 (S_0 \lambda_{\parallel})^{1/2}$ if $M_{A,0} < 1$ or $\Gamma_{\text{TMT}}^{w,q||} \propto M_{A,0}^3 (S_0 \lambda_{\parallel})^{1/2}$ if $M_{A,0} > 1$.
- Accounting for dynamic alignment (and tearing-mediated turbulence) introduces two breaks in the turbulent damping rate, instead of the single one that is present in the “classic” picture. For sub-Alfvénic turbulence, the first break corresponds to the transition scale between weak and strong turbulence (i.e., $\lambda_{\parallel} \sim M_{A,0}^4 \ell_0$ in terms of parallel wavelength of the AW packet), while it corresponds to the transition scale between isotropic and anisotropic turbulence for super-Alfvénic injection (i.e., $\lambda \sim M_{A,0}^3 \ell_0$). This is the same type of break that one would have in “classic” MHD turbulence. A second break, on the other hand, emerges due to the transition to tearing-mediated turbulence (which is only possible if dynamic alignment occurs), i.e., at a packet’s parallel wavelength $\lambda_{\parallel} \sim S_0^{-5/7} M_{A,0}^{8/7} \ell_0$ in sub-Alfvénic turbulence, or at $\lambda_{\parallel} \sim S_0^{-5/7} M_{A,0}^{-6/7} \ell_0$ for super-Alfvénic injection. (We recall that $M_{A,0}$ and S_0 are the Alfvénic Mach number of turbulent fluctuations and Lundquist number of the background plasma at injection scale ℓ_0 , respectively). Since CR “self-confinement” relies on a balance between the growth of these CR-driven Alfvén waves and their damping, it is reasonable to imagine that in astrophysical situations where turbulent damping is the most-relevant damping mechanism, these breaks would emerge also in the propagated CR spectrum (note that this is a simple damping-rate effect, and does not consider CR feedback on background fluctuations). It is thus interesting to mention that, assuming a Galactic magnetic field $B \sim 1\text{--}3 \mu\text{G}$ and an injection scale of background turbulence $\ell_0 \sim 30\text{--}100 \text{ pc}$, the above breaks in the damping rate could be translated to CR energies E_{CR} (assuming $\lambda_{\parallel} \sim r_L$, where r_L is the Larmor radius of the cosmic ray). A first break at $E_{\text{CR},1} \sim 10 \text{ TeV}$ would indeed emerge if the injection-scale Alfvénic Mach number $M_{A,0}$ of pre-existing turbulence is in the range $0.07 \lesssim M_{A,0} \lesssim 0.14$ (i.e., sub-

Alfvénic injection with $M_{A,0}$ of order ~ 0.1) or in the range $15 \lesssim M_{A,0} \lesssim 30$ (i.e., super-Alfvénic injection with $M_{A,0}$ of order ~ 10). Additionally, for both $M_{A,0}$ regimes determined above, a second break at CR energies $E_{CR,2} \sim 300$ GeV would be consistently recovered if the Lundquist number of the background plasma is of order $S_0 \sim 10^5$ – 10^7 . Clearly, this represents only an interesting feature in a very simplified scenario, and in general many other mechanisms that can affect CR transport may need to be taken into account (e.g., Fornieri et al. 2021; Lazarian and Xu 2021; Chernyshov et al. 2022; Kempfski and Quataert 2022; Kempfski et al. 2023; Lemoine 2023; Pezzi and Blasi 2024, and references therein).

It is worth concluding by stressing once more that the turbulent damping rates obtained in this work differ dramatically from the ones that are present in the literature even for “classic” MHD turbulence due to the confusion between χ^w and χ^z . All the existing CR studies that assume the turbulent damping rate as a fundamental ingredient in their calculations have thus employed an incorrect version of this damping rate. Hence, a number of previous works on CR self-confinement may need to be revised in view of the results presented here.

Acknowledgements. The author is grateful to the referee for several comments that helped to improve the manuscript. The author warmly acknowledges the kind hospitality of the Gran Sasso Science Institute (GSSI) in L’Aquila, and, in particular, Pasquale Blasi and Ottavio Fornieri, who introduced him to the paper by Farmer & Goldreich on turbulent damping during his first visit in November 2022. He also greatly acknowledges Alexandre Marcowith, Thierry Passot, and Steve Shore for helpful comments and feedback on the manuscript. The author is grateful to Stas Boldyrev, Ben Chandran, Matt Kunz, Alex Lazarian, Bill Matthaeus, Thierry Passot, Alex Schekochihin, and Pierre-Louis Sulem for useful conversations (and different opinions) about MHD turbulence theory over the years. This work has been partially supported by the French government, through the UCA^{JEDI} Investments in the Future project managed by the National Research Agency (ANR) with the reference number ANR-15-IDEX-01. The author is also supported by the ANR grant “MiCRO” with the reference number ANR-23-CE31-0016.

References

- Amato, E. (2011). The streaming instability: a review. *Mem. Soc. Astron. Italiana*, 82:806.
- Amato, E. and Blasi, P. (2018). Cosmic ray transport in the Galaxy: A review. *Adv. Space Res.*, 62(10):2731–2749.
- Bell, A. R. (2004). Turbulent amplification of magnetic field and diffusive shock acceleration of cosmic rays. *Mon. Not. R. Astron. Soc.*, 353(2):550–558.
- Berezinsky, V., Bulanov, S., Dogiel, V., and Ptuskin, V. (1990). *Astrophysics of cosmic rays*.
- Blasi, P., Amato, E., and Serpico, P. D. (2012). Spectral Breaks as a Signature of Cosmic Ray Induced Turbulence in the Galaxy. *Phys. Rev. Lett.*, 109(6):061101.
- Boldyrev, S. (2006). Spectrum of Magnetohydrodynamic Turbulence. *Phys. Rev. Lett.*, 96(11):115002.
- Boldyrev, S. and Loureiro, N. F. (2017). Magnetohydrodynamic Turbulence Mediated by Reconnection. *Astrophys. J.*, 844(2):125.
- Brandenburg, A. and Lazarian, A. (2013). Astrophysical Hydromagnetic Turbulence. *Space Sci. Rev.*, 178(2-4):163–200.
- Brunetti, G. and Jones, T. W. (2014). Cosmic Rays in Galaxy Clusters and Their Nonthermal Emission. *Int. J. Mod. Phys. D*, 23(4):1430007–98.
- Bruno, R. and Carbone, V. (2013). The Solar Wind as a Turbulence Laboratory. *Living Rev. Sol. Phys.*, 10.
- Cerri, S. S., Grošelj, D., and Franci, L. (2019). Kinetic plasma turbulence: recent insights and open questions from 3D3V simulations. *Front. Astron. Space Sci.*, 6:64.
- Cerri, S. S., Passot, T., Laveder, D., Sulem, P. L., and Kunz, M. W. (2022). Turbulent Regimes in Collisions of 3D Alfvén-wave Packets. *Astrophys. J.*, 939(1):36.
- Chandran, B. D. G. (2000). Scattering of Energetic Particles by Anisotropic Magnetohydrodynamic Turbulence with a Goldreich-Sridhar Power Spectrum. *Phys. Rev. Lett.*, 85(22):4656–4659.
- Chandran, B. D. G., Schekochihin, A. A., and Mallet, A. (2015). Intermittency and Alignment in Strong RMHD Turbulence. *Astrophys. J.*, 807(1):39.
- Chen, C. H. K. (2016). Recent progress in astrophysical plasma turbulence from solar wind observations. *J. Plasma Phys.*, 82(6):535820602.
- Chen, C. H. K., Mallet, A., Yousef, T. A., Schekochihin, A. A., and Horbury, T. S. (2011). Anisotropy of Alfvénic turbulence in the solar wind and numerical simulations. *Mon. Not. R. Astron. Soc.*, 415:3219–3226.
- Chernyshov, D. O., Dogiel, V. A., Ivlev, A. V., Erlykin, A. D., and Kiselev, A. M. (2022). Formation of the Cosmic-Ray Halo: The Role of Nonlinear Landau Damping. *Astrophys. J.*, 937(2):107.
- Cho, J. and Lazarian, A. (2002). Compressible Sub-Alfvénic MHD Turbulence in Low- β Plasmas. *Phys. Rev. Lett.*, 88(24):245001.
- Cho, J. and Lazarian, A. (2004). The Anisotropy of Electron Magnetohydrodynamic Turbulence. *Astrophys. J. Lett.*, 615:L41–L44.
- Cho, J. and Vishniac, E. T. (2000). The Anisotropy of Magnetohydrodynamic Alfvénic Turbulence. *Astrophys. J.*, 539(1):273–282.
- Elsässer, W. M. (1950). The Hydromagnetic Equations. *Phys. Rev.*, 79:183–183.
- Farmer, A. J. and Goldreich, P. (2004). Wave Damping by Magnetohydrodynamic Turbulence and Its Effect on Cosmic-Ray Propagation in the Interstellar Medium. *Astrophys. J.*, 604(2):671–674.
- Faucher-Giguère, C.-A. and Oh, S. P. (2023). Key Physical Processes in the Circumgalactic Medium. *Annu. Rev. Astronom. Astrophys.*, 61:131–195.
- Ferrière, K. (2020). Plasma turbulence in the interstellar medium. *Plasma Phys. Control. Fusion*, 62(1):014014.
- Fornieri, O., Gaggero, D., Cerri, S. S., De La Torre Luque, P., and Gabici, S. (2021). The theory of cosmic ray scattering on pre-existing MHD modes meets data. *Mon. Not. R. Astron. Soc.*, 502(4):5821–5838.
- Gaggero, D., Grasso, D., Marinelli, A., Urbano, A., and Valli, M. (2015). The Gamma-Ray and Neutrino Sky: A Consistent Picture of Fermi-LAT, Milagro, and IceCube Results. *Astrophys. J. Lett.*, 815(2):L25.
- Galtier, S., Nazarenko, S. V., Newell, A. C., and Pouquet, A. (2000). A weak turbulence theory for incompressible magnetohydrodynamics. *J. Plasma Phys.*, 63(5):447–488.
- Gary, S. P. (1993). *Theory of Space Plasma Microinstabilities*.
- Ginzburg, V. L. and Syrovatskii, S. I. (1964). *The Origin of Cosmic Rays*.
- Goldreich, P. and Sridhar, S. (1995). Toward a theory of interstellar turbulence. 2: Strong alfvénic turbulence. *Astrophys. J.*, 438:763–775.
- Holcomb, C. and Spitkovsky, A. (2019). On the Growth and Saturation of the Gyroresonant Streaming Instabilities. *Astrophys. J.*, 882(1):3.
- Horbury, T. S., Forman, M., and Oughton, S. (2008). Anisotropic Scaling of Magnetohydrodynamic Turbulence. *Phys. Rev. Lett.*, 101(17):175005.
- Iroshnikov, P. S. (1963). Turbulence of a Conducting Fluid in a Strong Magnetic Field. *Astron. Zh.*, 40:742.
- Ji, H. and Daughton, W. (2011). Phase diagram for magnetic reconnection in heliophysical, astrophysical, and laboratory plasmas. *Physics of Plasmas*, 18(11):111207–111207.
- Kempfski, P., Fielding, D. B., Quataert, E., Galishnikova, A. K., Kunz, M. W., Philippov, A. A., and Ripperda, B. (2023). Cosmic ray transport in large-amplitude turbulence with small-scale field reversals. *Mon. Not. R. Astron. Soc.*, 525(4):4985–4998.
- Kempfski, P. and Quataert, E. (2022). Reconciling cosmic ray transport theory with phenomenological models motivated by Milky-Way data. *Mon. Not. R. Astron. Soc.*, 514(1):657–674.
- Kolmogorov, A. N. (1941). Local structure of turbulence in incompressible viscous fluid at very large Reynolds numbers. *Dokl. Akad. Nauk SSSR*, 30:299.
- Kraichnan, R. H. (1965). Inertial-Range Spectrum of Hydromagnetic Turbulence. *Phys. Fluids*, 8:1385–1387.
- Kulsrud, R. and Pearce, W. P. (1969). The Effect of Wave-Particle Interactions on the Propagation of Cosmic Rays. *Astrophys. J.*, 156:445.
- Lazarian, A. (2016). Damping of Alfvén Waves by Turbulence and Its Consequences: From Cosmic-ray Streaming to Launching Winds. *Astrophys. J.*, 833(2):131.
- Lazarian, A., Vlahos, L., Kowal, G., Yan, H., Beresnyak, A., and de Gouveia Dal Pino, E. M. (2012). Turbulence, Magnetic Reconnection in Turbulent Fluids and Energetic Particle Acceleration. *Space Sci. Rev.*, 173(1-4):557–622.
- Lazarian, A. and Xu, S. (2021). Diffusion of Cosmic Rays in MHD Turbulence with Magnetic Mirrors. *Astrophys. J.*, 923(1):53.
- Lee, M. A. (1972). Cosmic-Ray Evolution due to Interactions with Self-Excited Plasma Waves. *Astrophys. J.*, 178:837–856.
- Lee, M. A. and Völk, H. J. (1973). Damping and Non-Linear Wave-Particle Interactions of Alfvén-Waves in the Solar Wind. *Ap&SS*, 24(1):31–49.
- Lemoine, M. (2023). Particle transport through localized interactions with sharp magnetic field bends in MHD turbulence. *J. Plasma Phys.*, 89(5):175890501.
- Lerche, I. and Schlickeiser, R. (2001). Cosmic ray transport in anisotropic magnetohydrodynamic turbulence. I. Fast magnetosonic waves. *Astron. Astrophys.*, 378:279–294.
- Mallet, A., Schekochihin, A. A., and Chandran, B. D. G. (2015). Refined critical balance in strong Alfvénic turbulence. *Mon. Not. R. Astron. Soc.*, 449:L77–L81.

- Mallet, A., Schekochihin, A. A., and Chandran, B. D. G. (2017). Disruption of sheet-like structures in Alfvénic turbulence by magnetic reconnection. *Mon. Not. R. Astron. Soc.*, 468:4862–4871.
- Mallet, A., Schekochihin, A. A., Chandran, B. D. G., Chen, C. H. K., Horbury, T. S., Wicks, R. T., and Greenan, C. C. (2016). Measures of three-dimensional anisotropy and intermittency in strong Alfvénic turbulence. *Mon. Not. R. Astron. Soc.*, 459(2):2130–2139.
- Marcowith, A., van Marle, A. J., and Plotnikov, I. (2021). The cosmic ray-driven streaming instability in astrophysical and space plasmas. *Phys. Plasmas*, 28(8):080601.
- Matthaeus, W. H., Servidio, S., Dmitruk, P., Carbone, V., Oughton, S., Wan, M., and Osman, K. T. (2012). Local Anisotropy, Higher Order Statistics, and Turbulence Spectra. *Astrophys. J.*, 750(2):103.
- Nava, L., Recchia, S., Gabici, S., Marcowith, A., Brahim, L., and Ptuskin, V. (2019). Non-linear diffusion of cosmic rays escaping from supernova remnants - II. Hot ionized media. *Mon. Not. R. Astron. Soc.*, 484(2):2684–2691.
- Ng, C. S. and Bhattacharjee, A. (1997). Scaling of anisotropic spectra due to the weak interaction of shear-Alfvén wave packets. *Phys. Plasmas*, 4(3):605–610.
- Oughton, S. and Matthaeus, W. H. (2020). Critical Balance and the Physics of Magnetohydrodynamic Turbulence. *Astrophys. J.*, 897(1):37.
- Pezzi, O. and Blasi, P. (2024). Galactic cosmic ray transport in the absence of resonant scattering. *Mon. Not. R. Astron. Soc.*, 529(1):L13–L18.
- Priest, E. and Forbes, T. (2007). *Magnetic Reconnection*.
- Quataert, E. and Gruzinov, A. (1999). Turbulence and Particle Heating in Advection-dominated Accretion Flows. *Astrophys. J.*, 520:248–255.
- Recchia, S., Galli, D., Nava, L., Padovani, M., Gabici, S., Marcowith, A., Ptuskin, V., and Morlino, G. (2022). Grammage of cosmic rays in the proximity of supernova remnants embedded in a partially ionized medium. *Astron. Astrophys.*, 660:A57.
- Ruszkowski, M. and Pfrommer, C. (2023). Cosmic ray feedback in galaxies and galaxy clusters. *Astron. Astrophys. Rev.*, 31(1):4.
- Sahraoui, F., Hadid, L., and Huang, S. (2020). Magnetohydrodynamic and kinetic scale turbulence in the near-Earth space plasmas: a (short) biased review. *RvMPP*, 4(1):4.
- Schekochihin, A. A. (2022). MHD turbulence: a biased review. *J. Plasma Phys.*, 88(5):155880501.
- Schekochihin, A. A. and Cowley, S. C. (2006). Turbulence, magnetic fields, and plasma physics in clusters of galaxies. *Phys. Plasmas*, 13(5):056501–056501.
- Schlickeiser, R. and Miller, J. A. (1998). Quasi-linear Theory of Cosmic-Ray Transport and Acceleration: The Role of Oblique Magnetohydrodynamic Waves and Transit-Time Damping. *Astrophys. J.*, 492(1):352–378.
- Schroer, B., Pezzi, O., Caprioli, D., Haggerty, C., and Blasi, P. (2021). Dynamical Effects of Cosmic Rays on the Medium Surrounding Their Sources. *Astrophys. J. Lett.*, 914(1):L13.
- Schroer, B., Pezzi, O., Caprioli, D., Haggerty, C. C., and Blasi, P. (2022). Cosmic-ray generated bubbles around their sources. *Mon. Not. R. Astron. Soc.*, 512(1):233–244.
- Shalchi, A. and Schlickeiser, R. (2004). Cosmic ray transport in anisotropic magnetohydrodynamic turbulence. III. Mixed magnetosonic and Alfvénic turbulence. *Astron. Astrophys.*, 420:799–808.
- Skilling, J. (1975). Cosmic ray streaming - III. Self-consistent solutions. *Mon. Not. R. Astron. Soc.*, 173:255–269.
- Teufel, A., Lerche, I., and Schlickeiser, R. (2003). Cosmic ray transport in anisotropic magnetohydrodynamic turbulence. II. Shear Alfvén waves. *Astron. Astrophys.*, 397:777–788.
- Weidl, M. S., Winske, D., and Niemann, C. (2019a). On the Background-gyroresonant Character of Bell’s Instability in the Large-current Regime. *Astrophys. J.*, 872(1):48.
- Weidl, M. S., Winske, D., and Niemann, C. (2019b). Three Regimes and Four Modes for the Resonant Saturation of Parallel Ion-beam Instabilities. *Astrophys. J.*, 873(1):57.
- Wicks, R. T., Horbury, T. S., Chen, C. H. K., and Schekochihin, A. A. (2010). Power and spectral index anisotropy of the entire inertial range of turbulence in the fast solar wind. *Mon. Not. R. Astron. Soc.*, 407:L31–L35.
- Xu, S. and Lazarian, A. (2022). Cosmic Ray Streaming in the Turbulent Interstellar Medium. *Astrophys. J.*, 927(1):94.
- Yan, H. and Lazarian, A. (2002). Scattering of Cosmic Rays by Magnetohydrodynamic Interstellar Turbulence. *Phys. Rev. Lett.*, 89(28):281102.
- Yan, H. and Lazarian, A. (2008). Cosmic-Ray Propagation: Nonlinear Diffusion Parallel and Perpendicular to Mean Magnetic Field. *Astrophys. J.*, 673(2):942–953.

Appendix A: Scaling of turbulent fluctuations at magnetohydrodynamic (MHD) scales

In this Appendix we briefly review the turbulent scaling of Alfvénic fluctuations at “fluid” (MHD) scales (see, e.g., [Schekochihin 2022](#), for a more detailed review on the topic). First, we present the standard scenario without scale-dependent alignment of turbulent fluctuations. In the second part, an alternative scenario in which such “dynamic alignment” is taking place in the critically balanced regime is presented.

In the following, isotropic injection will be assumed and ℓ_0 will denote the injection scale (i.e., the injection properties will not be affected by the presence of a mean magnetic-field direction \mathbf{B}_0 at that scale). Balanced injection will also be assumed, i.e., that the same amount of energy is injected in the Elsässer fields at ℓ_0 , $|\delta z_0^+|^2 \approx |\delta z_0^-|^2 = \delta z_0^2$. We thus define an injection-scale Alfvénic Mach number $M_{A,0} = \delta z_0 / v_{A,0} \approx \delta b_0 / B_0$, where $v_{A,0} = B_0 / \sqrt{4\pi\rho_0}$ is the Alfvén speed associated to the background plasma (having mass density ρ_0 and being embedded in a mean field \mathbf{B}_0). For isotropic injection, the nonlinear parameter at injection scales $\chi_0 = (k_{\perp,\text{inj}} \delta z_0) / (k_{\parallel,\text{inj}} v_{A,0})$ (see (4)) identifies with the injection-scale Alfvénic Mach number, i.e., $\chi_0 = M_{A,0}$. Analogously, we define the injection-scale Lundquist number $S_0 = \ell_0 v_{A,0} / \eta$, where η is the resistivity of the background plasma. The Lundquist and the Alfvénic Mach numbers can be combined to provide the (injection-scale) magnetic Reynolds number $Rm_0 = \ell_0 \delta z_0 / \eta = M_{A,0} S_0$.

An example of the resulting turbulent spectra and fluctuations’ anisotropy for different injection regimes and type of cascades are summarized in [Figures A.1 and A.2](#).

A.1. MHD turbulence without dynamic alignment

In this Section, we present what can be called as the “classic cascade” of Alfvénic fluctuations, i.e., the standard scenario in which a scale-dependent alignment of turbulent fluctuations is not taken into account. In this case, depending on the large-scale regime of injection, turbulence can start as either fluid-like ([Kolmogorov 1941](#)) or wave-like ([Ng and Bhattacharjee 1997](#); [Galtier et al. 2000](#)), until the point at which the cascade transitions into a critically balanced state ([Goldreich and Sridhar 1995](#)) and eventually reaches dissipation.

Sub- and Trans-Alfvénic injection ($M_{A,0} \leq 1$). When the injection conditions are isotropic and sub-Alfvénic, i.e., such that $\chi_0 = M_{A,0} < 1$, then fluctuations initially cascade in a weakly nonlinear regime. During that weak cascade only smaller perpendicular scales $\lambda_{\perp} < \ell_0$ are generated, while $\lambda_{\parallel} \sim \ell_0 \sim \text{const.}$ ⁹

⁹ This result is formally obtained through wave-turbulence theory ([Ng and Bhattacharjee 1997](#); [Galtier et al. 2000](#)). In weak MHD turbulence, the main contribution to the cascade is the three-wave interaction, where an Alfvén wave with frequency ω_1^{\mp} and wave-vector \mathbf{k}_1^{\mp} nonlinearly interacts with a counter-propagating Alfvén wave having frequency ω_2^{\mp} and wave-vector \mathbf{k}_2^{\mp} in order to generate a third wave with ω_3 and \mathbf{k}_3 . The resonance conditions for this process essentially correspond to “momentum” and “energy” conservation laws, namely $\mathbf{k}_1^{\pm} + \mathbf{k}_2^{\mp} = \mathbf{k}_3$ and $\omega_1^{\pm} + \omega_2^{\mp} = \omega_3$. Since for Alfvén waves these conditions on parallel wave-vectors become $k_{1,\parallel}^{\pm} - k_{2,\parallel}^{\mp} = \pm k_{3,\parallel}$ and $k_{1,\parallel}^{\pm} + k_{2,\parallel}^{\mp} = k_{3,\parallel}$, the only non-trivial solution requires that either $k_{2,\parallel}^{\mp} = 0$ and $k_{3,\parallel} = k_{1,\parallel}^{\pm}$, or $k_{1,\parallel}^{\pm} = 0$ and $k_{3,\parallel} = k_{2,\parallel}^{\mp}$. This means that the parallel wave-vector does not change during the three-wave interaction and only smaller perpendicular scales with $\mathbf{k}_{3,\perp} = \mathbf{k}_{1,\perp} + \mathbf{k}_{2,\perp}$ are generated by the weak cascade.

The cascade timescale in such weak regime is

$$\tau_{\text{casc},\lambda_{\perp}}^{(\text{subA})} \sim \frac{\tau_{\text{nl},\lambda_{\perp}}^{(\text{subA})}}{\chi_{\lambda_{\perp}}^{(\text{subA})}} \sim \frac{v_{A,0}}{\ell_0} \left(\frac{\lambda_{\perp}}{\delta z_{\lambda_{\perp}}^{(\text{subA})}} \right)^2, \quad (\text{A.1})$$

from which the fluctuations’ scaling in the inertial range are obtained by requiring a constant energy cascading rate ε through scales:

$$\frac{(\delta z_{\lambda_{\perp}}^{(\text{subA})})^2}{\tau_{\text{casc},\lambda_{\perp}}^{(\text{subA})}} \sim \varepsilon = \text{const.} \Rightarrow \frac{\delta z_{\lambda_{\perp}}^{(\text{subA})}}{v_{A,0}} \sim M_{A,0} \left(\frac{\lambda_{\perp}}{\ell_0} \right)^{1/2}, \quad (\text{A.2})$$

where we have used the fact that the cascading rate is constant through scales and thus it is the same as the injection rate, i.e., $\varepsilon \sim \varepsilon_0 \sim \delta z_0^2 / \tau_{\text{casc},0}^{(\text{subA})} \sim M_{A,0}^4 v_{A,0}^3 / \ell_0$. The fluctuations’ power spectrum is obtained as $\mathcal{E}_{\delta z} \sim (\delta z_{k_{\perp}})^2 / k_{\perp}$, and thus the one associated to the weak cascade is $\mathcal{E}_{\delta z}^{(\text{subA})}(k_{\perp}) \propto k_{\perp}^{-2}$ (here and in the following, we explicitly employ the more familiar wave-vector notation $k_{\perp} \sim \lambda_{\perp}^{-1}$ for the spectrum).

The weak cascade would reach a dissipation scale $\lambda_{\perp,\text{diss}}^{(\text{subA})}$ if the nonlinear timescale $\tau_{\text{nl},\lambda_{\perp}} \sim \lambda_{\perp} / \delta z_{\lambda_{\perp}}$ becomes comparable to the characteristic dissipation time $\tau_{\text{diss},\lambda_{\perp}} \sim \lambda_{\perp}^2 / \eta$, i.e.,

$$\frac{\lambda_{\perp,\text{diss}}^{(\text{subA})}}{\delta z_{\lambda_{\perp,\text{diss}}^{(\text{subA})}}} \sim \frac{(\lambda_{\perp,\text{diss}}^{(\text{subA})})^2}{\eta} \Rightarrow \frac{\lambda_{\perp,\text{diss}}^{(\text{subA})}}{\ell_0} \sim (M_{A,0} S_0)^{-2/3}. \quad (\text{A.3})$$

However, the scaling in (A.2) implies that the nonlinear parameter $\chi_{\lambda_{\perp}}$ increases with decreasing scales, i.e.,

$$\chi_{\lambda_{\perp}}^{(\text{subA})} \sim \frac{\ell_0 / v_{A,0}}{\lambda_{\perp}^{(\text{subA})} / \delta z_{\lambda_{\perp}}^{(\text{subA})}} \sim M_{A,0} \left(\frac{\lambda_{\perp}}{\ell_0} \right)^{-1/2}, \quad (\text{A.4})$$

and will thus achieve critical balance at a perpendicular scale

$$\chi_{\lambda_{\perp,\text{CB}}}^{(\text{subA})} \sim 1 \Rightarrow \frac{\lambda_{\perp,\text{CB}}}{\ell_0} \sim M_{A,0}^2. \quad (\text{A.5})$$

A transition to strong turbulence occurs only if $\lambda_{\perp,\text{CB}} \gg \lambda_{\perp,\text{diss}}^{(\text{subA})}$, and comparing (A.3) and (A.5), this means only if $S_0 \gg M_{A,0}^{-4}$. At scales below $\lambda_{\perp,\text{CB}}$ turbulence stays critically balanced and the cascade timescale identifies with the nonlinear time, i.e.,

$$\tau_{\text{casc},\lambda_{\perp} < \lambda_{\perp,\text{CB}}}^{(\text{subA})} \sim \tau_{\text{nl},\lambda_{\perp}}^{(\text{subA})} \sim \frac{\lambda_{\perp}}{\delta z_{\lambda_{\perp}}^{(\text{subA})}} \quad (\text{A.6})$$

As a result, the scaling of turbulent fluctuations at $\lambda_{\perp} < \lambda_{\perp,\text{CB}}$ is such that

$$\frac{(\delta z_{\lambda_{\perp} < \lambda_{\perp,\text{CB}}}^{(\text{subA})})^2}{\tau_{\text{nl},\lambda_{\perp} < \lambda_{\perp,\text{CB}}}^{(\text{subA})}} \sim \varepsilon = \text{const.} \Rightarrow \frac{\delta z_{\lambda_{\perp} < \lambda_{\perp,\text{CB}}}^{(\text{subA})}}{v_{A,0}} \sim M_{A,0}^{4/3} \left(\frac{\lambda_{\perp}}{\ell_0} \right)^{1/3}, \quad (\text{A.7})$$

while the critical-balance condition $\tau_{A,\lambda_{\perp}} \sim \tau_{\text{nl},\lambda_{\perp}}$ sets the scale-dependent anisotropy of turbulent fluctuations,

$$\frac{\lambda_{\parallel,\lambda_{\perp} < \lambda_{\perp,\text{CB}}}}{v_{A,0}} \sim \frac{\lambda_{\perp}}{\delta z_{\lambda_{\perp} < \lambda_{\perp,\text{CB}}}^{(\text{subA})}} \Rightarrow \frac{\lambda_{\parallel,\lambda_{\perp} < \lambda_{\perp,\text{CB}}}}{\ell_0} \sim M_{A,0}^{-4/3} \left(\frac{\lambda_{\perp}}{\ell_0} \right)^{2/3} \quad (\text{A.8})$$

Equation (A.8) implies that below $\lambda_{\perp,\text{CB}}$ the critically balanced cascade starts to generate also smaller parallel scales. From (A.7)

one can obtain a reduced (one-dimensional) perpendicular spectrum $\mathcal{E}_{\delta z}^{(\text{subA})}(k_{\perp} \lambda_{\perp, \text{CB}} > 1) \propto k_{\perp}^{-5/3}$ and a reduced parallel spectrum $\mathcal{E}_{\delta z}^{(\text{subA})}(k_{\parallel}) \propto k_{\parallel}^{-2}$.¹⁰ The above cascade eventually reaches dissipation at a scale $\lambda_{\perp, \text{diss}}^{(\text{subA})}$ for which the nonlinear and dissipation timescales become comparable, $\tau_{\text{nl}, \lambda_{\perp}}^{(\text{subA})} \sim \tau_{\text{diss}, \lambda_{\perp}}$, i.e.,¹¹

$$\frac{\lambda_{\perp, \text{diss}}^{(\text{subA})}}{\delta z_{\lambda_{\perp, \text{diss}}}^{(\text{subA})}} \sim \frac{(\lambda_{\perp, \text{diss}}^{(\text{subA})})^2}{\eta} \Rightarrow \frac{\lambda_{\perp, \text{diss}}^{(\text{subA})}}{\ell_0} \sim M_{\text{A},0}^{-1} S_0^{-3/4}. \quad (\text{A.9})$$

Super-Alfvénic injection ($M_{\text{A},0} > 1$). When fluctuations are injected (isotropically) with $\chi_0 = M_{\text{A},0} > 1$, the resulting turbulence starts as a strong “hydrodynamic-like” cascade, i.e., turbulence is isotropic and nearly insensitive to the presence of a background magnetic field for as long as $\delta b/B_0 > 1$ holds (that is, until the presence of a mean field starts to play a role in the cascade, at smaller scales). In the hydro-like range, fluctuations cascade with the nonlinear characteristic timescale,

$$\tau_{\text{casc}, \lambda}^{(\text{supA})} \sim \tau_{\text{nl}, \lambda}^{(\text{supA})} \sim \frac{\lambda}{\delta z_{\lambda}^{(\text{supA})}}, \quad (\text{A.10})$$

where λ is the isotropic wavelength of the fluctuations. The scaling for the fluctuating Elsässer variable immediately follow from the constancy of the energy cascade rate ε , i.e.,

$$\frac{(\delta z_{\lambda}^{(\text{supA})})^2}{\tau_{\text{nl}, \lambda}^{(\text{supA})}} \sim \varepsilon = \text{const.} \Rightarrow \frac{\delta z_{\lambda}^{(\text{supA})}}{v_{\text{A},0}} \sim M_{\text{A},0} \left(\frac{\lambda}{\ell_0} \right)^{1/3}, \quad (\text{A.11})$$

which corresponds to a Kolmogorov-like, isotropic fluctuations’ power spectrum $\mathcal{E}_{\delta z}^{(\text{supA})}(k) \propto k^{-5/3}$. This cascading regime goes on until it reaches dissipation, i.e., $\lambda_{\text{diss}}^{(\text{supA})} \sim (M_{\text{A},0} S_0)^{-3/4} \ell_0$. However, there is another important scale usually referred to as the “Alfvén scale” ℓ_{A} for which $\delta z_{\lambda}^{(\text{supA})} \sim v_{\text{A},0}$, given by

$$\frac{\ell_{\text{A}}}{\ell_0} \sim M_{\text{A},0}^{-3}, \quad (\text{A.12})$$

which is attained well before dissipation (i.e., $\ell_{\text{A}} \gg \lambda_{\text{diss}}^{(\text{supA})}$) only if $S_0 \gg M_{\text{A},0}^3$, and below which the cascade becomes critically balanced ($\chi_{\ell_{\text{A}}}^{(\text{supA})} \sim 1$) and thus anisotropic. Turbulent fluctuations at scales $\lambda_{\perp} < \ell_{\text{A}}$ thus follow the (GS95) scaling, i.e.,

$$\frac{\delta z_{\lambda_{\perp} < \ell_{\text{A}}}^{(\text{supA})}}{v_{\text{A},0}} \sim \left(\frac{\lambda_{\perp}}{\ell_{\text{A}}} \right)^{1/3} \sim M_{\text{A},0} \left(\frac{\lambda_{\perp}}{\ell_0} \right)^{1/3}, \quad (\text{A.13})$$

with a fluctuations’ wavelength anisotropy that now follows the relation $\lambda_{\parallel, \lambda_{\perp} < \ell_{\text{A}}} / \ell_0 \sim M_{\text{A},0}^{-1} (\lambda_{\perp} / \ell_0)^{2/3}$. This corresponds to reduced perpendicular and parallel power spectra at $k_{\perp} \ell_{\text{A}} \gtrsim 1$ that

¹⁰ There are different ways to obtain the reduced parallel spectrum, given the anisotropy in (A.8). One option is to invert the anisotropy relation to obtain the scaling of $\delta z_{k_{\parallel}} \propto k_{\parallel}^{-1/2}$, and then use the critical-balance condition to employ $\tau_{\text{A}, k_{\parallel}} \sim (k_{\parallel} v_{\text{A},0})^{-1}$ instead of τ_{nl} in the condition $(\delta z_{k_{\parallel}})^2 / \tau_{\text{A}, k_{\parallel}} \sim \varepsilon$. Another way is to use the condition that the total energy must be obtained by integrating both one-dimensional spectra independently, i.e., $\int dk_{\parallel} \mathcal{E}(k_{\parallel}) = E_{\text{tot}} = \int dk_{\perp} \mathcal{E}(k_{\perp})$, and using the anisotropy relation to rewrite $\mathcal{E}(k_{\perp})$ and dk_{\perp} .

¹¹ Here we implicitly assume that the condition $\lambda_{\perp, \text{diss}}^{(\text{subA})} \ll \lambda_{\perp, \text{CB}}$ holds also when the dissipation scale is computed using (A.9), which is indeed automatically fulfilled as long as $S_0 \gg M_{\text{A},0}^4$.

are $\propto k_{\perp}^{-5/3}$ and $\propto k_{\parallel}^{-2}$, respectively.

The dissipation scale $\lambda_{\perp, \text{diss}}^{(\text{supA})}$ in the super-Alfvénic regime is given again by matching the scale-dependent nonlinear timescale $\tau_{\text{nl}, \lambda_{\perp}}^{(\text{supA})}$ and the dissipation timescale $\tau_{\text{diss}, \lambda_{\perp}}$ for this type of cascade, i.e.,

$$\frac{\lambda_{\perp, \text{diss}}^{(\text{supA})}}{\delta z_{\lambda_{\perp, \text{diss}}}^{(\text{supA})}} \sim \frac{(\lambda_{\perp, \text{diss}}^{(\text{supA})})^2}{\eta} \Rightarrow \frac{\lambda_{\perp, \text{diss}}^{(\text{supA})}}{\ell_0} \sim (M_{\text{A},0} S_0)^{-3/4}. \quad (\text{A.14})$$

The condition $S_0 \gg M_{\text{A},0}^3$ ensures that the above scale is well below the Alfvén scale, i.e., $\lambda_{\perp, \text{diss}}^{(\text{supA})} \ll \ell_{\text{A}}$ (cf. (A.12) and (A.14)).

A.1.1. Summary of scaling for MHD turbulence without dynamic alignment

If one puts all the relations of Section A.1 back together, then the scaling for the (normalized) fluctuation amplitudes $\delta \hat{z} = \delta z / v_{\text{A},0}$ at MHD scales are the following. (We remind the reader that $\hat{\lambda}_{\perp} = \lambda_{\perp} / \ell_0$ is the normalized perpendicular wavelength).

$M_{\text{A},0} \leq 1$ regime (no dynamic alignment, $S_0 \gg M_{\text{A},0}^4$):

$$\delta \hat{z}_{\lambda_{\perp}}^{(\text{subA})} \sim \begin{cases} M_{\text{A},0} \hat{\lambda}_{\perp}^{1/2} & \hat{\lambda}_{\perp, \text{CB}} < \hat{\lambda}_{\perp} \leq 1 \quad [\text{W0}] \\ M_{\text{A},0}^{4/3} \hat{\lambda}_{\perp}^{1/3} & \hat{\lambda}_{\perp, \text{diss}}^{(\text{subA})} < \hat{\lambda}_{\perp} \leq \hat{\lambda}_{\perp, \text{CB}} \quad [\text{GS95}] \end{cases} \quad (\text{A.15})$$

where $\hat{\lambda}_{\perp, \text{CB}} \sim M_{\text{A},0}^2$ and $\hat{\lambda}_{\perp, \text{diss}}^{(\text{subA})} \sim M_{\text{A},0}^{-1} S_0^{-3/4}$, while the fluctuations’ anisotropy is given by

$$\hat{\lambda}_{\parallel, \hat{\lambda}_{\perp}}^{(\text{subA})} \sim \begin{cases} \text{const.} & \hat{\lambda}_{\perp, \text{CB}} < \hat{\lambda}_{\perp} \leq 1 \quad [\text{W0}] \\ M_{\text{A},0}^{-4/3} \hat{\lambda}_{\perp}^{2/3} & \hat{\lambda}_{\perp, \text{diss}}^{(\text{subA})} < \hat{\lambda}_{\perp} \leq \hat{\lambda}_{\perp, \text{CB}} \quad [\text{GS95}] \end{cases} \quad (\text{A.16})$$

where $\hat{\lambda}_{\parallel, \hat{\lambda}_{\perp}} = \lambda_{\parallel, \hat{\lambda}_{\perp}} / \ell_0$ is the normalized parallel wavelength of turbulent fluctuations.

$M_{\text{A},0} > 1$ regime (no dynamic alignment, $S_0 \gg M_{\text{A},0}^3$):

$$\delta \hat{z}_{\lambda_{\perp}}^{(\text{supA})} \sim \begin{cases} M_{\text{A},0} \hat{\lambda}_{\perp}^{1/3} & \hat{\ell}_{\text{A}} < \hat{\lambda}_{\perp} \leq 1 \quad [\text{K41}] \\ M_{\text{A},0} \hat{\lambda}_{\perp}^{1/3} & \hat{\lambda}_{\perp, \text{diss}}^{(\text{supA})} < \hat{\lambda}_{\perp} \leq \hat{\ell}_{\text{A}} \quad [\text{GS95}] \end{cases} \quad (\text{A.17})$$

where $\hat{\ell}_{\text{A}} \sim M_{\text{A},0}^{-3}$ and $\hat{\lambda}_{\perp, \text{diss}}^{(\text{supA})} \sim (M_{\text{A},0} S_0)^{-3/4}$, while fluctuations exhibit an anisotropy

$$\hat{\lambda}_{\parallel, \hat{\lambda}_{\perp}}^{(\text{supA})} \sim \begin{cases} \hat{\lambda}_{\perp} \sim \hat{\lambda} & \hat{\ell}_{\text{A}} < \hat{\lambda}_{\perp} \leq 1 \quad [\text{K41}] \\ M_{\text{A},0}^{-1} \hat{\lambda}_{\perp}^{2/3} & \hat{\lambda}_{\perp, \text{diss}}^{(\text{supA})} < \hat{\lambda}_{\perp} \leq \hat{\ell}_{\text{A}} \quad [\text{GS95}] \end{cases} \quad (\text{A.18})$$

with $\hat{\lambda}_{\parallel, \hat{\lambda}_{\perp}} = \lambda_{\parallel, \hat{\lambda}_{\perp}} / \ell_0$.

See Figures A.1 and A.2 for the resulting spectra and fluctuations’ anisotropy versus perpendicular wavenumber k_{\perp} .

A.2. MHD turbulence with scale-dependent alignment

In this Section, we present an alternative model to the ‘‘classic picture’’ of the Alfvénic cascade presented in Section A.1. In this case, after a hydrodynamic- or wave-like range, the cascade transitions into a critically balanced state in which fluctuations undergo a ‘‘dynamic’’ (i.e., scale-dependent) alignment process (Boldyrev 2006). Such dynamically aligned, critically balanced cascade can further transition into a so-called ‘‘tearing-mediated regime’’ at MHD scales (Boldyrev and Loureiro 2017; Mallet et al. 2017), before reaching the actual dissipation scales.

Sub- and Trans-Alfvénic injection ($M_{A,0} \leq 1$) with dynamic alignment. For isotropic and sub-Alfvénic injection, i.e., such that $\chi_0 = M_{A,0} < 1$, fluctuations initially develop a weak cascade following the same scaling as in (A.2). Dynamic alignment enters the picture only as soon as critical balance is reached, i.e., at scales $\lambda_\perp \leq \lambda_{\perp, \text{CB}} \sim M_{A,0}^2 \ell_0$: the idea behind this effect is that Elsässer fields tend to align in order to reduce the strength of nonlinearities.¹² Such process produces a scale-dependent angle between $\delta z_{\lambda_\perp}^+$ and $\delta z_{\lambda_\perp}^-$ that scales as

$$\sin \theta_{\lambda_\perp < \lambda_{\perp, \text{CB}}}^{(\text{subA})} \sim M_{A,0}^{-1/2} \left(\frac{\lambda_\perp}{\ell_0} \right)^{1/4}, \quad (\text{A.19})$$

which in turns appears explicitly in the nonlinear-time scaling, namely,

$$\tau_{\text{nl}, \lambda_\perp < \lambda_{\perp, \text{CB}}}^{(\text{subA})} \sim \frac{\lambda_\perp}{\delta z_{\lambda_\perp < \lambda_{\perp, \text{CB}}}^{(\text{subA})} \sin \theta_{\lambda_\perp < \lambda_{\perp, \text{CB}}}^{(\text{subA})}} \sim M_{A,0}^{1/2} \frac{\lambda_\perp^{3/4} \ell_0^{1/4}}{\delta z_{\lambda_\perp < \lambda_{\perp, \text{CB}}}^{(\text{subA})}} \quad (\text{A.20})$$

which decreases slower than the corresponding timescale when dynamic alignment is not present (cf. (A.6)). As a result, in the presence of a scale-dependent alignment, turbulent fluctuations at $\lambda_\perp < \lambda_{\perp, \text{CB}}$ scale as

$$\frac{\delta z_{\lambda_\perp < \lambda_{\perp, \text{CB}}}^{(\text{subA})}}{v_{A,0}} \sim M_{A,0}^{3/2} \left(\frac{\lambda_\perp}{\ell_0} \right)^{1/4} \quad (\text{A.21})$$

while the critical-balance condition $\tau_{A, \lambda_\perp} \sim \tau_{\text{nl}, \lambda_\perp < \lambda_{\perp, \text{CB}}}$ sets the scale-dependent anisotropy of dynamically aligned turbulent fluctuations,

$$\frac{\lambda_{\parallel, \lambda_\perp < \lambda_{\perp, \text{CB}}}}{\ell_0} \sim M_{A,0}^{-1} \left(\frac{\lambda_\perp}{\ell_0} \right)^{1/2}. \quad (\text{A.22})$$

Equation (A.22) implies that below $\lambda_{\perp, \text{CB}}$ a dynamically aligned, critically balanced cascade exhibits a stronger anisotropy than the corresponding cascade without a scale-dependent alignment.¹³ Using (A.21) one obtains the reduced perpendicular

¹² Another effect of dynamic alignment is that fluctuations exhibit three-dimensional anisotropy: if we call λ the length-scale of these 3D-anisotropic turbulent eddies in the direction perpendicular to both a mean-field $\langle \mathbf{B} \rangle_\lambda$ and magnetic-field fluctuations $\delta \mathbf{B}_{\perp, \lambda}$ at such scale ($\delta \mathbf{B}_{\perp, \lambda}$ being perpendicular to $\langle \mathbf{B} \rangle_\lambda$), then ℓ_λ and ξ_λ denote the length-scales along $\langle \mathbf{B} \rangle_\lambda$ and $\delta \mathbf{B}_{\perp, \lambda}$, respectively (Boldyrev 2006). In the following $k_\perp \sim \lambda_\perp^{-1}$ refers to the shortest length-scale λ , and we neglect the distinction between the two transverse directions $k_\lambda \sim \lambda^{-1}$ and $k_\xi \sim \xi^{-1}$; indeed an angular average of fluctuations’ properties in a wave-vector plane transverse to $\langle \mathbf{B} \rangle_\lambda$ would be dominated by the scaling with k_λ .

¹³ This scaling involves the parallel length-scale ℓ_λ and the shortest perpendicular length-scale λ . However, fluctuations are 3D-anisotropic. Since $\xi_\lambda \propto \lambda^{3/4}$ (Boldyrev 2006), the anisotropy scales as $\ell_\xi \propto \xi^{2/3}$, when considering the longest perpendicular length-scale ξ .

spectrum $\mathcal{E}_{\delta z}^{(\text{subA})}(k_\perp > k_{\perp, \text{CB}}) \propto k_\perp^{-3/2}$, which is slightly shallower than the $-5/3$ obtained without dynamic alignment; on the other hand, the parallel spectrum is still $\mathcal{E}_{\delta z}^{(\text{subA})}(k_\parallel) \propto k_\parallel^{-2}$.

At this point, if the Lundquist number is ‘‘not large enough’’ (i.e., such that $S_0 \lesssim M_{A,0}^{-4}$; see later), this dynamically aligned, critically balanced cascade will reach the dissipation scale $\lambda_{\perp, \text{diss}}^{(\text{subA})}$ when $\tau_{\text{nl}, \lambda_\perp} \sim \tau_{\text{diss}, \lambda_\perp}$. Using (A.20), this means

$$\frac{\lambda_{\perp, \text{diss}}^{(\text{subA})}}{\ell_0} \sim (M_{A,0} S_0)^{-2/3}. \quad (\text{A.23})$$

However, in most cases of interest, the Lundquist number S_0 is large enough that this critically balanced cascade of dynamically aligning fluctuations transitions to a ‘‘tearing-mediated’’ cascade. Such transition occurs at a perpendicular scale $\lambda_{\perp, *}$ for which the timescale associated to the (linear) growth rate of the tearing instability, $\gamma_{\lambda_\perp}^t \sim S_0^{-1/2} (\lambda_\perp / \ell_0)^{-3/2} (\delta z_{\lambda_\perp} / v_{A,0})^{1/2} (v_{A,0} / \ell_0)$, becomes comparable to the eddy turnover time at that scale $\tau_{\text{nl}, \lambda_\perp}^{(\text{subA})} \sim \lambda_\perp / \delta z_{\lambda_\perp}^{(\text{subA})}$, i.e., $\gamma_{\lambda_\perp}^t \tau_{\text{nl}, \lambda_\perp}^{(\text{subA})} \sim 1$, yielding

$$\frac{\lambda_{\perp, *}^{(\text{subA})}}{\ell_0} \sim M_{A,0}^{-2/7} S_0^{-4/7}. \quad (\text{A.24})$$

Comparing (A.24) and (A.23), one finds that a tearing-mediated range emerges only if $S_0 \gg M_{A,0}^{-4}$, so that $\lambda_{\perp, *}^{(\text{subA})} \gg \lambda_{\perp, \text{diss}}^{(\text{subA})}$. In this regime, the generation of turbulent fluctuations at scales $\lambda_\perp \leq \lambda_{\perp, *}$ is due to the disruption of the (dynamically aligning¹⁴) turbulent eddies by magnetic reconnection; hence, the scale $\lambda_{\perp, *}$ is usually referred to as the ‘‘disruption scale’’. Thus the tearing instability timescale $\tau_{\lambda_\perp}^t \sim 1/\gamma_{\lambda_\perp}^t$ is the ‘‘cascade time’’ in this range of scales¹⁵, and assuming a constant energy flux through scales, $(\delta z_{\lambda_\perp < \lambda_{\perp, *}}^{(\text{subA})})^2 / \tau_{\lambda_\perp}^t \sim \varepsilon = \text{const.}$, provides with the fluctuations’ scaling in the tearing-mediated regime:

$$\frac{\delta z_{\lambda_\perp < \lambda_{\perp, *}}^{(\text{subA})}}{v_{A,0}} \sim S_0^{1/5} M_{A,0}^{8/5} \left(\frac{\lambda_\perp}{\ell_0} \right)^{3/5}, \quad (\text{A.25})$$

corresponding to a reduced spectrum $\mathcal{E}_{\delta z}^{(\text{subA})}(k_\perp > k_{\perp, *}) \propto k_\perp^{-11/5}$. Due to the nonlinear stage of the tearing instability, turbulent fluctuations in the reconnection-mediated range tend to misalign in a scale-dependent fashion, following the scaling¹⁶

$$\sin \theta_{\lambda_\perp < \lambda_{\perp, *}}^{(\text{subA})} \sim S_0^{-3/5} M_{A,0}^{-4/5} \left(\frac{\lambda_\perp}{\ell_0} \right)^{-4/5}, \quad (\text{A.26})$$

while fluctuations’ anisotropy in this range is obtained from the CB-like condition $\gamma_{\lambda_\perp}^t \tau_{A, \lambda_\perp} \sim 1$, i.e.,

$$\frac{\lambda_{\parallel, \lambda_\perp < \lambda_{\perp, *}}}{\ell_0} \sim S_0^{2/5} M_{A,0}^{-4/5} \left(\frac{\lambda_\perp}{\ell_0} \right)^{6/5}. \quad (\text{A.27})$$

The tearing-mediated cascade eventually dissipates at a scale where the characteristic dissipation time becomes comparable with the tearing timescale, namely,

$$\gamma_{\lambda_\perp}^t \tau_{\text{diss}, \lambda_\perp} \sim 1 \Rightarrow \frac{\lambda_{\perp, \text{diss}}^{(\text{subA})}}{\ell_0} \sim M_{A,0}^{-1} S_0^{-3/4}. \quad (\text{A.28})$$

¹⁴ We remark that a tearing-mediated regime fundamentally relies on the fact that turbulent fluctuations develop anisotropy in the plane perpendicular to a mean field (viz., $\lambda \ll \xi_\lambda$). Hence, tearing-mediated turbulence only exists if fluctuations do align in a scale-dependent fashion.

¹⁵ One can verify *a posteriori* that in this regime fluctuations’ scaling indeed preserves the condition $\tau_{\text{nl}, \lambda_\perp} \sim 1/\gamma_{\lambda_\perp}^t$ at all scales below $\lambda_{\perp, *}$.

¹⁶ This is obtained as the ratio between the resistive inner scale δ and the longitudinal scale ζ of the current layer (Boldyrev and Loureiro 2017).

which, interestingly enough, is exactly the same dissipation scale (A.9) that was found for the (GS95) cascade.

Super-Alfvénic injection ($M_{A,0} > 1$) with dynamic alignment.

In this regime, the cascade develops in a hydrodynamic-like fashion until the Alfvén scale $\ell_A \sim M_{A,0}^{-3} \ell_0$, i.e., without being affected by dynamic alignment. Thus fluctuations follow the scaling in (A.11) down to ℓ_A , and only below such scale the cascade becomes critically balance and dynamic alignment plays a role. At $\lambda_\perp < \ell_A$, the fluctuations' alignment angle scales as

$$\sin \theta_{\lambda_\perp < \ell_A}^{(\text{supA})} \sim M_{A,0}^{3/4} \left(\frac{\lambda_\perp}{\ell_0} \right)^{1/4}, \quad (\text{A.29})$$

and the nonlinear time at such scales is thus given by

$$\tau_{\text{nl}, \lambda_\perp < \ell_A}^{(\text{supA})} \sim \frac{\lambda_\perp}{\delta z_{\lambda_\perp < \ell_A}^{(\text{supA})} \sin \theta_{\lambda_\perp < \ell_A}^{(\text{supA})}} \sim M_{A,0}^{-3/4} \frac{\lambda_\perp^{3/4} \ell_0^{1/4}}{\delta z_{\lambda_\perp < \ell_A}^{(\text{supA})}}. \quad (\text{A.30})$$

As a result, in the presence of a scale-dependent alignment, turbulent fluctuations at $\lambda_\perp < \ell_A$ scale as

$$\frac{(\delta z_{\lambda_\perp < \ell_A}^{(\text{supA})})^2}{\tau_{\text{nl}, \lambda_\perp < \ell_A}^{(\text{supA})}} \sim \varepsilon = \text{const.} \Rightarrow \frac{\delta z_{\lambda_\perp < \ell_A}^{(\text{supA})}}{v_{A,0}} \sim M_{A,0}^{3/4} \left(\frac{\lambda_\perp}{\ell_0} \right)^{1/4} \quad (\text{A.31})$$

corresponding to a $\propto k_\perp^{-3/2}$ spectrum for $k_\perp \ell_A > 1$. Fluctuations' scale-dependent anisotropy is obtained via the critical-balance condition $\tau_{A, \lambda_\perp < \ell_A} \sim \tau_{\text{nl}, \lambda_\perp < \ell_A}$, i.e.,

$$\frac{\lambda_{\parallel, \lambda_\perp < \ell_A}}{\ell_0} \sim M_{A,0}^{-3/2} \left(\frac{\lambda_\perp}{\ell_0} \right)^{1/2}. \quad (\text{A.32})$$

The above cascade of critically balanced, dynamically aligned fluctuations can either reach actual dissipation at a scale $\lambda_{\perp, \text{diss}}^{(\text{supA})} / \ell_0 \sim M_{A,0}^{-1} S_0^{-2/3}$, or, if $S_0 \gg M_{A,0}^3$ holds, will instead transition to the tearing-mediated regime at a (disruption) scale¹⁷

$$\frac{\lambda_{\perp, *}}{\ell_0} \sim M_{A,0}^{-9/7} S_0^{-4/7}. \quad (\text{A.33})$$

At scales $\lambda_\perp < \lambda_{\perp, *}$, fluctuations will then follow the scaling

$$\frac{\delta z_{\lambda_\perp < \lambda_{\perp, *}}^{(\text{supA})}}{v_{A,0}} \sim S_0^{1/5} M_{A,0}^{6/5} \left(\frac{\lambda_\perp}{\ell_0} \right)^{3/5}, \quad (\text{A.34})$$

corresponding to a $\propto k_\perp^{-11/5}$ spectrum at $k_\perp \lambda_{\perp, *}^{(\text{supA})} > 1$. In this range, fluctuations develop a scale-dependent (mis-)alignment angle

$$\sin \theta_{\lambda_\perp < \lambda_{\perp, *}}^{(\text{supA})} \sim S_0^{-3/5} M_{A,0}^{-3/5} \left(\frac{\lambda_\perp}{\ell_0} \right)^{-4/5}, \quad (\text{A.35})$$

and an anisotropy given by

$$\frac{\ell_{\parallel, \lambda_\perp < \lambda_{\perp, *}}}{\ell_0} \sim S_0^{2/5} M_{A,0}^{-3/5} \left(\frac{\lambda_\perp}{\ell_0} \right)^{6/5}. \quad (\text{A.36})$$

Finally, this tearing-mediated regime reaches dissipation at

$$\frac{\lambda_{\perp, \text{diss}}^{(\text{supA})}}{\ell_0} \sim \frac{\eta^{3/4}}{\varepsilon^{1/4} \ell_0} \sim (M_{A,0} S_0)^{-3/4}. \quad (\text{A.37})$$

¹⁷ We remind the reader that the transition scale in (A.33) is obtained using the condition $\gamma_{\lambda_{\perp, *}}^t \tau_{\text{nl}, \lambda_{\perp, *}}^{(\text{supA})} \sim 1$, where the growth rate of the tearing instability is given by $\gamma_{\lambda_{\perp, *}}^t \sim S_0^{-1/2} (\lambda_\perp / \ell_0)^{-3/2} (\delta z_{\lambda_\perp} / v_{A,0})^{1/2} (v_{A,0} / \ell_0)$.

A.2.1. Summary of scaling for MHD turbulence with dynamic alignment

We summarize here all the scaling of Section A.2 for the (normalized) fluctuation amplitudes $\delta \hat{z} = \delta z / v_{A,0}$ with respect to the (normalized) perpendicular wavelength $\hat{\lambda}_\perp = \lambda_\perp / \ell_0$.

$M_{A,0} \leq 1$ regime (with dynamic alignment, $S_0 \gg M_{A,0}^{-4}$):

$$\delta \hat{z}_{\hat{\lambda}_\perp}^{(\text{subA})} \sim \begin{cases} M_{A,0} \hat{\lambda}_\perp^{1/2} & \hat{\lambda}_{\perp, \text{CB}} < \hat{\lambda}_\perp \leq 1 \quad [\text{W0}] \\ M_{A,0}^{3/2} \hat{\lambda}_\perp^{1/4} & \hat{\lambda}_{\perp, *}^{(\text{subA})} < \hat{\lambda}_\perp \leq \hat{\lambda}_{\perp, \text{CB}} \quad [\text{B06}] \\ S_0^{1/5} M_{A,0}^{8/5} \hat{\lambda}_\perp^{3/5} & \hat{\lambda}_{\perp, \text{diss}}^{(\text{subA})} < \hat{\lambda}_\perp \leq \hat{\lambda}_{\perp, *}^{(\text{subA})} \quad [\text{TMT}] \end{cases} \quad (\text{A.38})$$

with $\hat{\lambda}_{\perp, \text{CB}} \sim M_{A,0}^2$, $\hat{\lambda}_{\perp, *}^{(\text{subA})} \sim M_{A,0}^{-2/7} S_0^{-4/7}$, and $\hat{\lambda}_{\perp, \text{diss}}^{(\text{subA})} \sim M_{A,0}^{-1} S_0^{-3/4}$, while the fluctuations' anisotropy is given by

$$\hat{\lambda}_{\parallel, \hat{\lambda}_\perp}^{(\text{subA})} \sim \begin{cases} \text{const.} & \hat{\lambda}_{\perp, \text{CB}} < \hat{\lambda}_\perp \leq 1 \quad [\text{W0}] \\ M_{A,0}^{-1} \hat{\lambda}_\perp^{1/2} & \hat{\lambda}_{\perp, *}^{(\text{subA})} < \hat{\lambda}_\perp \leq \hat{\lambda}_{\perp, \text{CB}} \quad [\text{B06}] \\ S_0^{2/5} M_{A,0}^{-4/5} \hat{\lambda}_\perp^{6/5} & \hat{\lambda}_{\perp, \text{diss}}^{(\text{subA})} < \hat{\lambda}_\perp \leq \hat{\lambda}_{\perp, *}^{(\text{subA})} \quad [\text{TMT}] \end{cases} \quad (\text{A.39})$$

where $\hat{\lambda}_{\parallel, \hat{\lambda}_\perp} = \lambda_{\parallel, \hat{\lambda}_\perp} / \ell_0$ is the normalized parallel wavelength of turbulent fluctuations.

$M_{A,0} > 1$ regime (with dynamic alignment, $S_0 \gg M_{A,0}^3$):

$$\delta \hat{z}_{\hat{\lambda}_\perp}^{(\text{supA})} \sim \begin{cases} M_{A,0} \hat{\lambda}^{1/3} & \hat{\ell}_A < \hat{\lambda} \leq 1 \quad [\text{K41}] \\ M_{A,0}^{3/4} \hat{\lambda}_\perp^{1/4} & \hat{\lambda}_{\perp, *}^{(\text{supA})} < \hat{\lambda}_\perp \leq \hat{\ell}_A \quad [\text{B06}] \\ S_0^{1/5} M_{A,0}^{6/5} \hat{\lambda}_\perp^{3/5} & \hat{\lambda}_{\perp, \text{diss}}^{(\text{supA})} < \hat{\lambda}_\perp \leq \hat{\lambda}_{\perp, *}^{(\text{supA})} \quad [\text{TMT}] \end{cases} \quad (\text{A.40})$$

where $\hat{\ell}_A \sim M_{A,0}^{-3}$, $\hat{\lambda}_{\perp, *}^{(\text{supA})} \sim M_{A,0}^{-9/7} S_0^{-4/7}$, and $\hat{\lambda}_{\perp, \text{diss}}^{(\text{supA})} \sim (M_{A,0} S_0)^{-3/4}$, while the fluctuations' anisotropy is given by

$$\hat{\lambda}_{\parallel, \hat{\lambda}_\perp}^{(\text{supA})} \sim \begin{cases} \hat{\lambda}_\perp \sim \hat{\lambda} & \hat{\ell}_A < \hat{\lambda} \leq 1 \quad [\text{K41}] \\ M_{A,0}^{-3/2} \hat{\lambda}_\perp^{1/2} & \hat{\lambda}_{\perp, *}^{(\text{supA})} < \hat{\lambda}_\perp \leq \hat{\ell}_A \quad [\text{B06}] \\ S_0^{2/5} M_{A,0}^{-3/5} \hat{\lambda}_\perp^{6/5} & \hat{\lambda}_{\perp, \text{diss}}^{(\text{supA})} < \hat{\lambda}_\perp \leq \hat{\lambda}_{\perp, *}^{(\text{supA})} \quad [\text{TMT}] \end{cases} \quad (\text{A.41})$$

with $\hat{\lambda}_{\parallel, \hat{\lambda}_\perp} = \lambda_{\parallel, \hat{\lambda}_\perp} / \ell_0$.

See Figures A.1 and A.2 for the resulting spectra and fluctuations' anisotropy versus perpendicular wavenumber k_\perp .

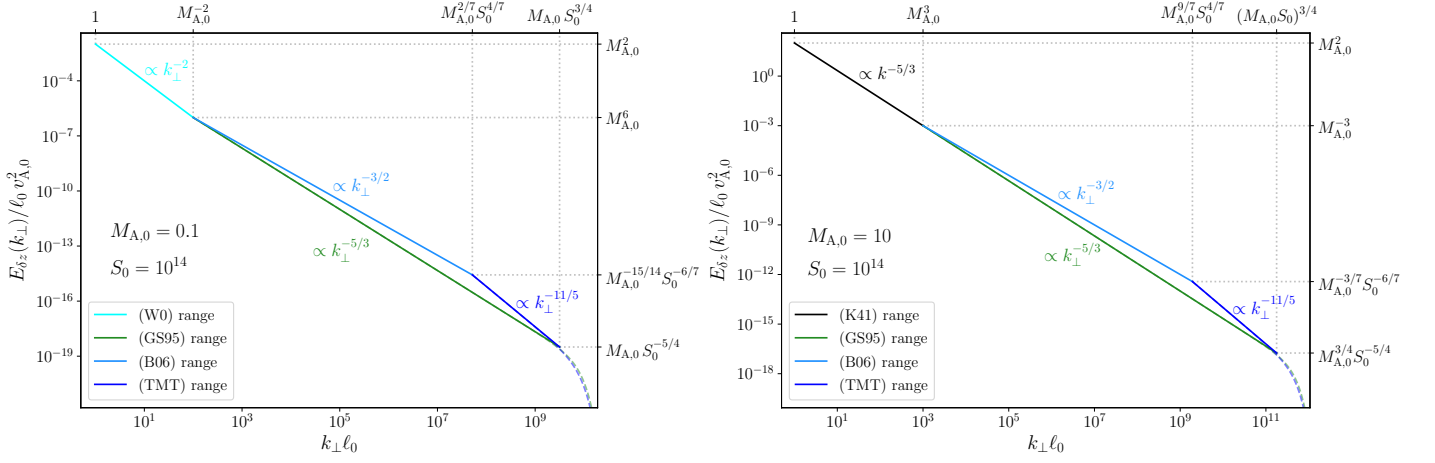


Fig. A.1: Normalized reduced spectrum, $E_{\delta z}(k_{\perp})/\ell_0 v_{A,0}^2$, versus fluctuations' perpendicular wave-vector, $k_{\perp} \ell_0$, in a plasma with Lunquist number $S_0 = 10^{14}$ and sub-Alfvénic ($M_{A,0} = 0.1$, left) or super-Alfvénic ($M_{A,0} = 10$, right) injection regimes. Different colors represent different cascading regimes (see legend), and general expressions for transition scales and fluctuations' power level are reported on the right and upper axis. Solid lines show ideal scaling from (A.15), (A.17), (A.38), and (A.40) for the nominal range $\ell_0^{-1} \lesssim k_{\perp} \lesssim \lambda_{\perp, \text{diss}}^{-1}$, while dashed lines represent their extension in the dissipation range with a damping factor $\sim \exp(-k_{\perp}^2 \lambda_{\perp, \text{diss}}^2)$.

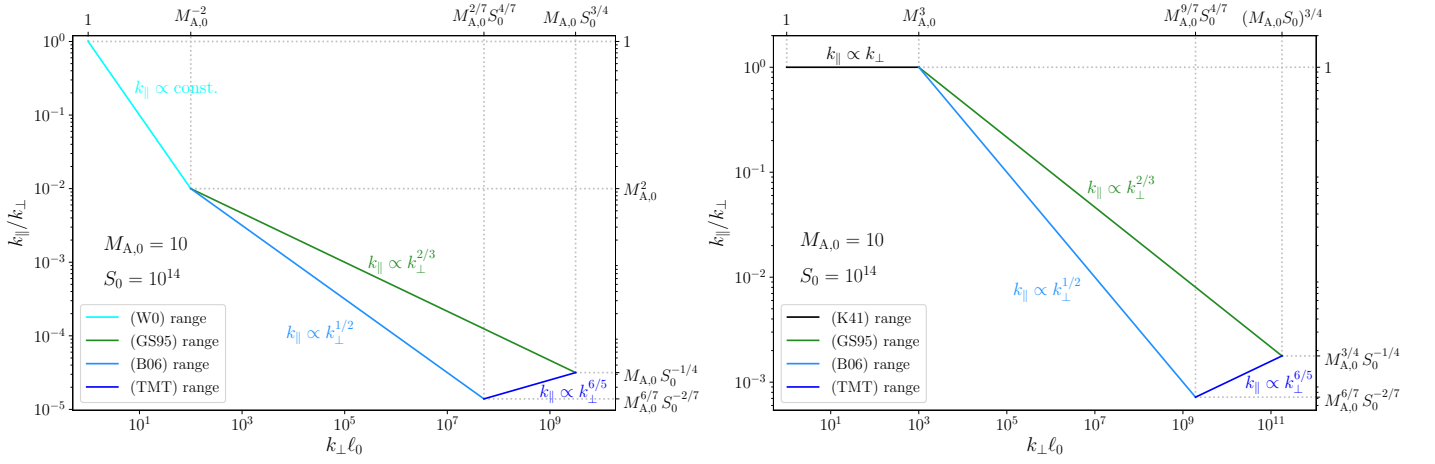


Fig. A.2: Wave-vector anisotropy of fluctuations, k_{\parallel}/k_{\perp} , versus normalized fluctuations' perpendicular wave-vector, $k_{\perp} \ell_0$, for the cascades shown in Figure A.1 in the nominal range $\ell_0^{-1} \lesssim k_{\perp} \lesssim \lambda_{\perp, \text{diss}}^{-1}$ (cf. equations (A.16), (A.18), (A.39), and (A.41)).